Modeling net sheet-flow sediment transport rate under skewed and asymmetric oscillatory flows over a sloping bed

Jing Yuan[a], Weikai Tan[a]

[a]*Department of Civil and Environmental Engineering, National University of Singapore, 1 Engineering Dr. 2, Block E1A 07-03, Singapore 117576*

Abstract

A one-dimensional-vertical model is developed for net sheet-flow sediment transport rate under oscillatory boundary layer flows. This model couples the boundary-layer model proposed by Yuan and Madsen (2015) with new predictors for bedload and suspended-load transport rates. Sediment concentration is modeled by solving the advection-diffusion equation with a parameterized turbulence diffusivity and a bottom pick-up rate. The slope effect is included in the predictions of instantaneous bedload transport rate and sediment pick-up rate, so the model can rigorously account for wave nonlinearity (velocity skewness and asymmetry) together with a mild bottom slope. The model performance on net sediment transport rate is excellent for large grain sizes, except that the velocity-asymmetry effect seems to be moderately underestimated. For small grain sizes, the model performance deteriorates, but is still acceptable for many cases. This is possibly because the model does not consider turbulence damping due to stratification and underestimates the phase-lag effect. Using the validated model, it is found that a boundary layer streaming due to velocity skewness and/or asymmetry

can be a major contributor to net transport rate, when significant sediment suspension occurs. A simple case study also suggests that a mild bottom slope can be equally important as the wave nonlinearity for producing net sediment transport rate. Model predictions show that wave-nonlinear and bottom-slope effects can be linearly superimposed, which provides a simple way for incorporating bottom slope into existing transport-rate formulas.
Keywords: sheet flow, sediment transport, bottom slope, theoretical model, boundary layer streaming

1. Introduction

Sediment transport is directly related to beach erosion and scour of coastal structures, and therefore is of primary interest to coastal scientists and engineers. Under very strong flow conditions, e.g. storm waves in shallow waters, intense sediment motion occurs in the immediate vicinity of a dynamically plane bed, which is often referred to as sheet-flow sediment transport. A number of previous studies, e.g. Wilson (1987) and Sumer et al. (1996), suggest that the thickness of sheet-flow layer is scaled with the product of sediment diameter and certain characteristics Shield parameter, and therefore can be only a few mm to a few cm. For wave-induced sheet flows, the net (time-averaged) transport rate is of the top importance, and therefore attracts a substantial amount of research efforts over the past decades (reviewed by Ribberink et al., 2008). A near-bed wave orbital motion with two symmetric half-periods cannot produce a net transport rate over a horizontal bed, so a non-zero net transport rate is due to some factors that introduce a small imbalance between the two wave half-periods.

Wave nonlinearity is believed to be a key factor. Shoaling waves become increasingly nonlinear as they travel into shallow waters, and the nonlinearity makes the bottom oscillatory flow skewed (the onshore half-period has a larger peak velocity but shorter duration than the offshore one) and asymmetric (the velocity time series has a "sawtooth" shape). If sediment transport rate is assumed to vary with flow condition in a quasi-steady manner, velocity skewness makes the total transport under the onshore half-period larger than that under the offshore half-period, leading to a net onshore transport rate. This is often referred to as the wave-shape effect. A number of sheet-flow experiments with skewed flows in oscillatory water tunnel (OWT) (e.g. Dibajnia and Watanabe, 1992; Ribberink and Al-Salem, 1994) have been conducted, and an onshore transport rate is indeed observed for tests with medium or coarse sediment grains. However, for fine sediments, a net offshore sediment transport rate is observed in many tests (e.g. Dibajnia and Watanabe, 1992; O'Donoghue and Wright, 2004). The phase-lag effect (e.g. Dohmen-Janssen et al., 2002) is believed to be the main reason, i.e. sediments suspended during the onshore half-period cannot settle back to the movable bed before the flow reversal, which significantly enhances the suspended-load transport during the offshore half-period. Velocity asymmetry, according to Nielsen (1992), makes the boundary layer under the onshore half-period thinner than that under the offshore half-period. Consequently, the vertical velocity gradient and bottom shear stress under the onshore half-period is larger. This argument is supported by some recently boundary-layer-flow experiments (e.g. van der A et al., 2011). Such a wave-shape effect will possibly lead to a net onshore transport rate, which is indeed observed in a few OWT

sheet-flow experiments (e.g. van der A et al., 2010). Some observations of near-bed sediment concentration (e.g. Watanabe and Sato, 2004) suggests that the phase-lag effects may further enhance the onshore net transport rate for purely asymmetric oscillatory flows. This is because the sediment settling time before flow reversal is shorter for the offshore half-period, so the phase-lag effect can better benefit the suspended-load transport under the onshore half-period.

Many process-based model have been proposed for predicting net sheet-flow sediment transport rate due to skewness and asymmetry. Most of them are based on the 1-dimensional-vertical (1DV) approximation, i.e. flow is uniform in the bottom-parallel direction (as in OWTs), and adopt the one-phase approach (e.g. Davies and Li, 1997; Hassan and Ribberink, 2010), which treats suspended sediments as passive tracers. The main difference among existing models is the closure of turbulent fluid stress, e.g. from simple mixing-length-based theories (e.g. Styles and Glenn, 2000) to more complicated one-equation (e.g. Villaret and Davies, 1995) and two-equation (e.g. Hassan and Ribberink, 2010) closure models. High sediment concentration damps local turbulent and leads to hindered setting of sediments, so modifications of turbulent closure schemes and parameters for sediment diffusivity have been incorporated into various one-phase modeling techniques (e.g. Davies and Li, 1997; Guizien et al., 2003). Ruessink et al. (2009) investigated the effects of skewness and asymmetry on net transport rate under realistic field conditions. Recently, Caliskan and Fuhrman (2017) extended an 1DV and one-phase model to graded sands. To better describe the sediment motion in the sheet-flow layer, two-phase models are becoming popular (e.g. Hsu

and Hanes, 2004; Liu and Sato, 2006; Li et al., 2008). These models differ in turbulence closure schemes, closures of sediment-phase turbulent stresses and fluid-sediment interactions. The reader is referred to the reviews by Amoudry et al. (2008) and Kranenburg et al. (2013a) for more in-depth discussions. High-fidelity numerical models are still too computationally expensive to be integrated into large-scale nearshore models for coastal hydrodynamics and sediment transport, so it is desirable to develop simple yet realistic model that can balance computational efficiency and model accuracy.

Skewness and asymmetry differentiate the flow turbulence between the two half-periods, which leads to a boundary layer streaming (TI-streaming hereafter) embedded in the oscillatory flow (e.g. Trowbridge and Madsen, 1984). Within the wave boundary layer, TI-streaming usually opposites the wave traveling direction, and therefore can produce an offshore net transport rate. In OWTs, it is balanced by a facility-generated current, resulting in an offshore-oriented residual mean velocity in the very near-bottom region (e.g Ribberink and Al-Salem, 1995). Yuan and Madsen (2015) showed that TI-streaming is quite strong for purely skewed oscillatory flows, but is very weak for purely asymmetric oscillatory flows. This streaming is different from another well-known wave boundary layer streaming first proposed by Longuet-Higgins (1953) (LH-streaming hereafter), which is associated with wave propagation. The LH-streaming is usually in the wave traveling (onshore) direction, so it works against the TI-streaming. A substantial amount of work has been done to account for the LH-streaming in numerical modeling sheet-flow sediment transport (e.g. Fuhrman et al., 2013; Yu et al., 2010; Kranenburg et al., 2013b) or some empirical transport-rate formulas (e.g.

van der A et al., 2013). However, very little work has been done to investigate the TI-streaming's contribution, although it has been shown that they can be equally important for determining the mean Eulerian velocity (e.g Kranenburg et al., 2012).

In coastal regions, the seabed usually has a mild bottom slope with the downslope direction being offshore. The bottom-parallel component of gravity force can increase the total sediment transport during the offshore half-period but reduce that for the onshore half-periods, so a net offshore (downslope) transport rate can be expected. Although this effect is well recognized, very little work has been done for a good quantitative understanding. King (1991) in his OWT study measured how average sediment transport rate under a half-period of sinusoidal flow varies with bottom slope. Recently, Yuan et al. (2017) reported another experimental study in which net sheet-flow sediment transport rate is measured under sinusoidal oscillatory flows in a sloped OWT. They showed that the net downslope transport rate increases linearly with bottom slope and developed a simple model to illustrate the experimental results. Based on their measurements, they argued that the bottom-slope-induced net transport rate can be as important as those due to skewness or asymmetry. More research effort is required to further justify this argument. Most theoretical models assume a horizontal seabed, so the bottom-slope effect is rarely modeled in a process-based manner. Thus, it is also of interest to model the effect of nonlinear wave shape together with a sloping bed.

The main objective of this study is to investigate the relative importance of TI-streaming and bottom slope for modeling net sediment transport rate,

which is not well understood to date. To this end, a process-based model is developed by extending the model proposed by Yuan et al. (2017), so it can rigorously account for a mild bottom slope together with velocity skewness and/or asymmetry. The outline of this paper is as follows. Section 2 presents the model, which is validated in Section 3. The importance of TI-streaming and bottom slope for net transport rate is discussed in Section 4 through some computational experiments. Conclusions are provided in Section 5.

2. A process-based model for net sheet-flow sediment transport rate

In this study, we assume that the flow is uniform in the bottom-parallel direction, which is strictly satisfied for OWT flows, so the governing equations for momentum and sediment suspension are 1DV. It should be noted that the LH-streaming, which comes from the convective acceleration terms in the governing equation, is consequently excluded in our model. This, however, does not defeat the main objectives of this study. The semi-analytical model developed by Yuan and Madsen (2015) (YM15 hereafter) is adopted for modeling turbulent oscillatory boundary layers. Net sediment transport rate is modeled as the sum of bedload and suspended-load components. Model descriptions are provided in the following sub-sections.

2.1. Boundary layer flow

Yuan and Madsen (2015) developed a semi-analytical model for turbulent oscillatory boundary layer flows with (or without) a collinear current. Following the 1DV approximation, the governing equation for Reynolds-averaged

bottom-parallel velocity component, u, is

$$\frac{\partial u}{\partial t} = -\frac{1}{\rho}\frac{\partial p}{\partial x} + \frac{\partial}{\partial z}\left(\nu_T \frac{\partial u}{\partial z}\right) \tag{1}$$

where ρ is water density, t is time, p is water pressure, x and z are the bottom-parallel and bottom-normal coordinates, respectively, and ν_T is the turbulent eddy viscosity. The pressure gradient is related to the free-stream flow based on the boundary-layer approximation

$$\frac{\partial u_\infty}{\partial t} = -\frac{1}{\rho}\frac{\partial p}{\partial x} \tag{2}$$

where u_∞ is the free-stream oscillatory velocity. In their model, ν_T is expressed as a time-averaged value $\nu_{T0}(z)$ times a temporal variation function $f(t)$, i.e.

$$\nu_T = \nu_{T0}(z) f(t) \tag{3}$$

where $\nu_{T0}(z)$ is described by a four-layer vertical structure (see Appendix A), and $f(t)$ is approximated by a Fourier series. The model is driven by an oscillatory free-stream velocity described by a Fourier series

$$u_\infty(t) = \sum\nolimits_n U_{b,n} \cos(n\omega t + \varphi_{\infty,n}) \tag{4}$$

where $U_{b,n}$ and $\varphi_{\infty,n}$ are the n-harmonic amplitude and phase, respectively. For skewed or asymmetric oscillatory flows in OWTs, Yuan and Madsen (2015) showed that the period-averaged mean velocity u_0 is the cancellation of a TI-streaming u_{0s} and a facility-generated return current u_{0c}, i.e. $u_0 = u_{0s} + u_{0c}$. Thus, the prediction of u_0 requires a reference value at a reference level, i.e.

$$u_0 = u_{cr} \quad \text{at} \quad z = z_{cr} \tag{5}$$

Eqs. (4) and (5) prescribe the wave and the current conditions, respectively, so with the knowledge of bottom roughness k_b, which determines the no-slip bottom boundary condition at $z = z_0 = k_b/30$, Eq. (1) can be solved in a semi-analytical manner. By benchmarking against a variety of OWT experiments, including asymmetric or skewed oscillatory flows, it is demonstrated that the model can accurately predict bottom shear stress and Reynolds-averaged velocity. Thus, it is a powerful tool for understanding the boundary layer processes in OWTs.

Under sheet-flow conditions, the intense sediment-fluid interaction leads to an increase of flow resistance, which is reflected by an enhanced bottom roughness. In this study, we adopt the movable bed roughness proposed by Herrmann and Madsen (2007), i.e.

$$k_m = \left[4.5 \max\left(\psi_{wm} - \psi_{cr}, 0\right) + 1.7\right] d_{50} \tag{6}$$

where d_{50} is the sediment median diameter, ψ_{cr} is the critical Shield parameter for incipient motion, and ψ_{wm} is the Shields parameter related to the maximum wave bottom shear stress, i.e.

$$\psi_{wm} = \frac{{u_{*wm}}^2}{(s-1)gd_{50}} = \frac{f_w {U_b}^2}{2(s-1)gd_{50}} \tag{7}$$

where s is sediment specific density and g is gravitational acceleration. In this study, we only consider periodic oscillatory flows. The wave nonlinearity (represented by the higher-order harmonics in the free-stream velocity) is usually weak and therefore can be neglected for determining ψ_{wm}, so U_b is simply taken as the first-harmonic $U_{b,1}$ of the free-stream velocity, and the friction factor f_w is evaluated using the following formula proposed by

Humbyrd (2012)

$$f_w = \exp\left[5.70\left(\frac{A_{b1}}{k_b}\right)^{-0.101} - 7.46\right], 10 < \frac{A_{b1}}{k_b} < 10^5 \tag{8}$$

where $A_{b,1} = U_{b,1}/\omega$ is the first-harmonic excursion amplitude. Since $k_b = k_m$ in Eq. (8), Eqs. (6) to (8) are evaluated iteratively for k_m. The YM15 model is subsequently applied with the total bottom roughness $k_b = k_m$, which is hereafter referred to as the total-flow prediction. The turbulent eddy viscosity and flow velocity from the total-flow prediction will be subsequently used for predicting net suspended-load transport rate.

As will be introduced later, the prediction of bedload transport rate requires an effective bottom shear stress, $\tau_{be}(t)$, based on an effective bottom roughness $k_e = d_{50}$, and the bottom boundary condition for sediment suspension requires an skin-friction bottom shear stress, $\tau_b'(t)$, which is based on a skin roughness $k_s = 2.5d_{50}$. The skin-friction concept proposed by Madsen (2002) is adopted here to obtain $\tau_{be}(t)$ and $\tau_b'(t)$. From the total-flow prediction, we first obtain a predicted mean velocity at the level δ_k (see Appendix A), where current becomes dominant. With this new reference mean velocity and the free-stream oscillatory velocity, the YM15 model is subsequently applied with k_b=k_e (or k_s) to obtain the required predictions.

2.2. Net bedload transport rate

The net bedload transport rate is obtained by time-averaging the intra-period prediction. Since sediment grains moving as bedload transport can almost immediately response to the change of flow condition, the instantaneous bedload transport rate $q_{SB}(t)$ on a sloping bed is predicted in a

quasi-steady manner with the Madsen (1993) conceptual bedload model, i.e.

$$q_{SB}(t) = \frac{8}{\tan\phi_m(s-1)gF_m(\beta(t))} \max\left[u_{*e}(t)^2 - u_{*cr}^2 F_s(\beta(t)), 0\right] \cdot \left(u_{*e}(t) - u_{*cr}\sqrt{\frac{F_m(\beta(t))}{2}}\right) \frac{\tau_{be}(t)}{|\tau_{be}(t)|} \tag{9}$$

with

$$F_m(\beta(t)) = \cos\beta(t)\left(1 + \frac{\tan\beta(t)}{\tan\phi_m}\right) \tag{10}$$

and

$$F_s(\beta(t)) = \cos\beta(t)\left(1 + \frac{\tan\beta(t)}{\tan\phi_s}\right) \tag{11}$$

In Eqs. (9) to (11), $u_{*cr} = \sqrt{\tau_{bcr}/\rho}$ is the shear velocity related to the critical bottom shear stress, τ_{bcr}, for incipient motion, $\phi_m = 28°$ is the moving friction angle, $\phi_s = 47°$ is the static friction angle, $u_{*e}(t) = \sqrt{|\tau_{be}(t)|/\rho}$ is the instantaneous shear velocity associated with the effective bottom shear stress $\tau_{be}(t)$, $\beta(t)$ is the instantaneous bottom slope, which takes the value

$$\beta(t) = \begin{cases} \beta, \tau_{be}(t) > 0 \quad \text{(upslope)} \\ -\beta, \tau_{be}(t) \leq 0 \quad \text{(downslope)} \end{cases} \tag{12}$$

where β is the absolute value of bottom slope and the upslope direction is defined as the positive direction of $\tau_{be}(t)$. To be consistent with the assumptions leading to the Madsen (1993) model, $\tau_{be}(t)$ is predicted based a bottom roughness $k_b = d_{50}$. The net bedload transport rate $q_{B,net}$ is eventually calculated by period-averaging $q_{SB}(t)$.

2.3. Suspended-load transport rate

The net suspended-load transport rate is modeled by depth-integrating the mean sediment flux $\Phi(z)$, which can be written as

$$q_{S,net} = \int_{z_s}^{\infty} \Phi(z)dz = \int_{z_s}^{\infty} \overline{uc}dz \tag{13}$$

where z_s is a reference level defining the bottom of suspended-load layer and the overbar indicates period averaging. We can express both flow velocity u and sediment concentration c as Fourier series, i.e.

$$u(z,t) = u_0 + U_1(z)\cos(\omega t + \varphi_{U1}) + U_2(z)\cos(2\omega t + \varphi_{U2}) + ... \tag{14}$$

and

$$c(z,t) = c_0 + c_1(z)\cos(\omega t + \varphi_{c1}) + c_2(z)\cos(2\omega t + \varphi_{c2}) + ... \tag{15}$$

where u_0 and c_0 are the mean values of velocity and concentration, respectively, U_i and φ_{Ui} are the amplitude and the phase of i-th-harmonic velocity, and c_i and φ_{ci} are the amplitude and the phase of i-th-harmonic concentration. Eq. (13) can then be written as

$$q_{S,net} = q_{S0,net} + q_{Sw,net} = \int_{z_s}^{\infty} \Phi_0(z)dz + \int_{z_s}^{\infty} \Phi_w(z)dz \tag{16}$$

where

$$\Phi_0 = u_0 c_0 \tag{17}$$

is the mean sediment flux associated with the mean flow and

$$\Phi_w = \sum_{i=1}^{\infty} \Phi_i = \sum_{i=1}^{\infty} \frac{1}{2} U_i c_i \cos(\varphi_{ci} - \varphi_{Ui}) \tag{18}$$

is the mean sediment flux associated with the oscillatory flow with Φ_i being the mean sediment flux due to the i-th harmonic physics. In Eq. (16), $q_{S0,net}$ is the mean-flow-related part of net suspended-load transport rate and $q_{Sw,net}$ can be taken as the wave-related part. The convective velocity is from the total-flow prediction of the YM15 model, so the remaining task is solving for sediment concentration.

The 1DV advection-diffusion equation for $c(z,t)$ is

$$\frac{\partial c}{\partial t} = w_s \frac{\partial c}{\partial z} + \frac{\partial}{\partial z}\left(D_T \frac{\partial c}{\partial z}\right) \tag{19}$$

where w_s is the sediment fall velocity obtained using the formula proposed by Jimenez and Madsen (2003) and D_T is the turbulence sediment diffusivity. Following Yuan et al. (2017), D_T is parameterized based on the turbulent eddy viscosity, ν_T, from the total-flow prediction, which essentially assumes that the turbulence associated with total flow resistance mixes sediments. Many experimental and numerical studies suggest that the stratification effect due to sediment suspension damps turbulence within the boundary layer, and hence makes D_T smaller than ν_T, while the centripetal effect of eddies might lead to a D_T larger than ν_T. Herrmann and Madsen (2007) showed that these two effects may cancel each other, so ν_T can be modeled without considering turbulence damping and D_T is simply equal to ν_T. For simplicity, our model follows their implication, and the consequences will be discussed later. To allow analytical solution for Eq. (19), D_T is further assumed to be time-invariant and takes the value of ν_{T0}, except that the exponential-decaying layer in Eq. (A.1) is ignored. This layer usually does not exist unless the current is extremely weak, and neglecting it will simplify the analytical solution. Thus, D_T can be expressed as

$$D_T = \begin{cases} \kappa u_{*wc} z, & z_r \le z < \delta_I \\ \kappa u_{*wc} \delta_I, & \delta_I \le z < \delta_c \\ \kappa u_{*c} z, & z \le \delta_c \end{cases} \tag{20}$$

where κ is the von Karman constant, z_r is a reference level for specifying a bottom boundary condition, u_{*wc} and u_{*c} are combined wave-current shear

velocity and current shear velocity, respectively, δ_I is a transition level with the wave boundary layer (see appendix A), and δ_c is the level where $D_T = \kappa u_{*c} z$ intersects with the lower two-layer structure, which is further limited by the wave boundary layer thickness δ_w

$$\delta_c = \min(\delta_w, \frac{u_{*wc}}{u_{*c}} \delta_I) \tag{21}$$

Definition sketch for D_T is provided in Fig. 1. The parameters in Eq. (20) and (21) are from total-flow prediction with the YM15 model. Eq. (19) can be solved harmonic-by-harmonic, i.e. the n-th-harmonic equation is

$$in\omega c^{(n)} = w_s \frac{\partial c^{(n)}}{\partial z} + \frac{\partial}{\partial z}\left(D_T \frac{\partial c^{(n)}}{\partial z} \right) \tag{22}$$

We here introduce a normalized vertical coordinate

$$\xi = \frac{z}{l}, \quad l = \frac{\kappa u_{*wc}}{\omega} \tag{23}$$

where l is the characteristic length scale of the oscillatory boundary layer. The following set of generic equations are obtained

$$\begin{cases} inc^{(n)} = a\frac{\partial c^{(n)}}{\partial \xi} + \frac{\partial}{\partial \xi}\left(\xi \frac{\partial c^{(n)}}{\partial \xi} \right), & \xi_r \le \xi < \xi_I \\ inc^{(n)} = a\frac{\partial c^{(n)}}{\partial \xi} + \xi_I \frac{\partial^2 c^{(n)}}{\partial \xi^2}, & \xi_I \le \xi < \xi_c \\ inc^{(n)} = a\frac{\partial c^{(n)}}{\partial \xi} + \frac{\partial}{\partial \xi}\left(r_{wc} \xi \frac{\partial c^{(n)}}{\partial \xi} \right), & \xi_c \le \xi \end{cases} \tag{24}$$

where $r_{wc} = u_{*c}/u_{*wc}$, $(\xi_r, \xi_I, \xi_c) = (z_r, \delta_I, \delta_c)/l$ and

$$a = \frac{w_s}{\kappa u_{*wc}} \tag{25}$$

is the Rouse parameter. Analytical solution of Eq. (24), which satisfies that

$c(n) \to 0$ as $z \to \infty$, is

$$c^{(n)} = \begin{cases} A\xi^{-a/2}[\mathrm{ker}_a(2\sqrt{n\xi}) + i\mathrm{kei}_a(2\sqrt{n\xi})] \\ \quad + B\xi^{-a/2}[\mathrm{ber}_a(2\sqrt{n\xi}) + i\mathrm{bei}_a(2\sqrt{n\xi})], \quad \xi_r \le \xi < \xi_I \\ C\exp\left(\frac{-a+\sqrt{a^2+4in\xi_I}}{2\xi_I}\xi\right) \\ \quad + D\exp\left(\frac{-a-\sqrt{a^2+4in\xi_I}}{2\xi_I}\xi\right), \quad \xi_I \le \xi < \xi_c \\ E\xi^{\frac{-a}{2r_{wc}}}[\mathrm{ker}_{a/r_{wc}}(2\sqrt{n\xi/r_{wc}}) + i\mathrm{kei}_{a/r_{wc}}(2\sqrt{n\xi/r_{wc}})], \quad \xi_c \le \xi \end{cases} \tag{26}$$

where (ker_v, kei_v, ber_v, bei_v) are Kelvin's functions of order v. To quantify the five integral constants, A to E, four equations are determined by matching predictions of $c^{(n)}$ and $D_T\partial c^{(n)}/\partial z$ at ξ_I and ξ_c, and the fifth equation is given by matching a bottom boundary condition at the reference level, $z = z_r$ or $\xi = \xi_r$. Here we choose to specify the bottom condition as a sediment pick-up rate, i.e. a n-th harmonic sediment pick-up rate $P(n)$ for the n-th harmonic solution, which gives

$$\left.\frac{\partial c^{(n)}}{\partial \xi}\right|_{\xi=\xi_r} = \frac{-lP^{(n)}}{D_T(z_r)} \tag{27}$$

The mean sediment concentration c_0 is described by

$$w_s c_0 + D_T\frac{\partial c_0}{\partial z} = 0 \tag{28}$$

The analytical solution, which also satisfies that the mean concentration vanishes as $z \to \infty$, is

$$\bar{c} = \begin{cases} \frac{lP_0\xi_r}{aD_T(z_r)}\left(\frac{\xi}{\xi_r}\right)^{-a}, \quad \xi_r \le \xi < \xi \\ \frac{lP_0\xi_r}{aD_T(z_r)}\left(\frac{\xi_I}{e\xi_r}\right)^{-a}\exp\left(-a\frac{\xi}{\xi_I}\right), \quad \xi_I \le \xi < \xi_c \\ \frac{lP_0\xi_r}{aD_T(z_r)}\left(\frac{\xi_I}{e\xi_r}\right)^{-a}\exp\left(-a\frac{\xi_c}{\xi_I}\right)\left(\frac{\xi}{\xi_c}\right)^{-a/r_{wc}}, \quad \xi_c \le \xi \end{cases} \tag{29}$$

where P_0 is the mean sediment pick-up rate. $P^{(n)}$ and P_0 in Eqs. (27) and (29) are determined as follows. For sediment transport in steady flows, a balance between sediment pick-up and settling is satisfied at the level where a bottom reference concentration, c_b, is specified, i.e.

$$P = w_s c_b \quad \text{at} \quad z = z_r \tag{30}$$

c_b is commonly related to bottom shear stress, which represents the local turbulence. Thus, P can be simply related to bottom shear stress through a formula for c_b. In this study, the following formula proposed by Zyserman and Fredsøe (1994) is adopted

$$c_b = \frac{0.331(\max[\psi' - \psi_{cr}, 0])^{1.75}}{1 + 0.72(\max[\psi' - \psi_{cr}, 0])^{1.75}}, \quad z_r = 2d_{50} \tag{31}$$

Where ψ' is a skin Shields parameter associated with a skin bottom shear stress τ_b' based on a roughness $k_s = 2.5d_{50}$, i.e.

$$\psi' = \frac{{\tau_b}'}{\rho(s-1)gd_{50}} \tag{32}$$

Assuming that P varies with ψ' in a quasi-steady manner, a time-varying P on a horizontal bed is obtained with Eqs. (30), (31) and a time-varying $\psi'(t)$ obtained through the aforementioned skin-friction calculation using the YM15 model.

2.4. The effect of bottom slope

On a sloping bed, the bottom-parallel gravity force affects the incipient motion for sediment grains. By examining the force balance of a single sediment grain, Madsen (1991) derived a bottom-slope modification for critical

Shields parameter. For a small bottom slope (a few degrees), which is generally applicable for field conditions, the modified Shield parameter is

$$\psi_{cr,\beta}(t) = \psi_{cr} \cos\beta(t) \left(1 + \frac{\tan\beta(t)}{\tan\phi_s}\right) \tag{33}$$

where $\beta(t)$ takes the same sign as $\psi'(t)$. As discussed by Yuan et al. (2017), c_b is proportional to the amount of sediment grains moving as bedload, so it varies with bottom slope as $c_b(\beta) = c_b(0) \cdot (1 - \tan\beta/\tan\phi_m)$, where $c_b(0)$ is for a horizontal bed. Thus, the slope effect on P is also a factor of $(1 - \tan\beta/\tan\phi_m)$, according to Eq (30), so $P(t)$ can be expressed as

$$P(t) = w_s \cdot \frac{0.331(\max[\psi'(t) - \psi_{cr,\beta}(t), 0])^{1.75}}{1 + 0.72(\max[\psi'(t) - \psi_{cr,\beta}(t), 0])^{1.75}} \cdot \left[1 - \frac{\tan\beta(t)}{\tan\phi_m}\right] \tag{34}$$

The obtained $P(t)$ is numerically Fourier analyzed to give $P^{(n)}$ and P_0 for the analytical solution of sediment concentration.

2.5. Reference level for suspended-load

A critical question for our model is how to define the lower boundary for the suspended-load layer, i.e. the integral limit z_s in Eq. (13). There is no clear boundary separating bedload and suspended-load layers for the sheet-flow regime. A natural choice following the definition of sediment pick-up rate is $z_s = z_r = 2d_{50}$. However, jumping bedload sediment grains can reach much higher levels than twice the sediment diameter, so adopting $z_s = 2d_{50}$ possibly will double count something already considered as bedload transport. It can be expected that this problem is important for coarse-sand scenarios, i.e. the sediment suspension will be limited to a very thin near-bed layer. In the work of Yuan et al. (2017), which adopts $z_s = 2d_{50}$, they need to

significantly reduce the reference concentration for modeling their coarse-sand tests, which essentially eliminates the suspended-load prediction, but the reduced reference concentration at $z_s = 2d_{50}$ can be extremely low and therefore unrealistic. A common definition for the upper limit of sheet-flow layer is where the sediment concentration is below 0.08, which is a threshold value for neglecting interactions among sand grains. Based on many OWT measurements, Ribberink et al. (2008) proposed that the maximum sheet-flow layer thickness $\delta_{s,max}$ under sinusoidal oscillatory flow can be given by

$$\frac{\delta_{s,\max}}{d_{50}} = 10.6\theta_{\max} \tag{35}$$

where θ_{max} is a Shields parameter calculated with d_{50} and the free-stream oscillatory flow (see their section 2.2). In this study, we take z_s as the period-averaged thickness of the sheet-flow layer, which is simply assumed to be half of $\delta_{s,\max}$ evaluated with Eq. (35), i.e.

$$\frac{z_s}{d_{50}} = \max(2, 5.3\theta_{\max}) \tag{36}$$

where θ_{max} is estimated with the first-harmonic free-stream velocity. Using this z_s will exclude the sediment transport rate within the very near-bed layer with extremely high concentration, which, to some extent, prevents double-counting what has already been covered in bedload prediction.

3. Model validation

Our conceptual model does not directly resolve the sheet-flow layer, which creates a problem for model validation in the very near-bed region. In our model, $z = 0$ can be considered as the instantaneous no-motion level, but in

most experiments the reference level is the initial no-motion level. Therefore, a level z' in experiments is effectively $z = z' + \delta_e(t)$ in our model prediction, where $\delta_e(t)$ is the instantaneous erosion depth. This difference is illustrated with the definition sketches in Fig. 2. Previous studies, e.g. O'Donoghue and Wright (2004), showed that δ_e is a function of sediment diameter and flow condition, and can be a few millimeters. Consequently, it is unreasonable to compare predictions with measurements within $z \sim O(mm)$ for time-varying quantities. At higher levels, i.e. $z \gg \delta_e(t)$, this problem becomes insignificant. In view of this, the validation for the prediction of flow velocity and sediment concentration will be limited to period-averaged quantities only. After that, model-data comparisons for net sediment transport rate will be presented, followed by some discussions.

3.1. Period-averaged sediment concentration and velocity

The model-data comparisons are based on two OWT tests with skewed oscillatory flows, one (C1) is the condition 1 reported by Ribberink and Al-Salem (1995) and the other (FA7515 as shown in Fig. 3a) is reported by O'Donoghue and Wright (2004). The free-stream velocity for both tests is specified as

$$u_\infty(t) = U_{\infty,1}\cos(\omega t) + U_{\infty,2}\cos(2\omega t) \tag{37}$$

The detailed test conditions are summarized in Table 1. C1 is with medium sand (d_{50}=0.21mm), while FA7515 is with fine sand (d_{50}=0.13mm).

The predictions of mean velocity u_0 are presented in Fig. 4. The model reasonably captures that u_0 is negative in the very near-bed region but becomes positive at higher levels. The model-data agreement for test C1 is quite

good, while for test FA7515, the model underestimates the negative near-bed u_0 from z=0.5 to 3.5 cm by up to 45%. As discussed by Yuan and Madsen (2015), u_0 for skewed oscillatory flows in OWTs is a very small residue due to the cancellation of TI-streaming u_{0s} and return current u_{0c}. For this case, the magnitudes of u_{0s} and u_{0c} are about 20 cm/s. Although underestimating their difference by up to 4 cm/s seems alerting, it implies a quite slight underestimate of u_{0s} (less than 10-20%), so the net suspended-load transport rate due to TI-streaming can still be reasonably predicted.

The prediction of mean sediment concentration c_0 is presented in Fig. 5. Here only the measurements outside the sheet-flow layer are considered. The model accurately predicts c_0 for test C1, but heavily overestimates c_0 for test FA7515. Test C1 has a weaker flow condition and larger sediment grain size than test FA7515, so its sediment concentration is very low, i.e. c_0 is within O(0.01$\sim$1 g/l). The effect of flow stratification can therefore be neglected, as assumed in our model. However, the fine-sand test FA7515 has high values of c_0, which quickly decreases from O(100 g/l) to O(10 g/l) in the bottom-most 2 cm layer. It can be hypothesized that such a high sediment concentration gradient leads to a significant stratification, which dramatically damps the local turbulence. As a result, our model overestimates the turbulence-induced suspension. Following Herrmann and Madsen (2007), turbulence damping can be represented by a flux Richardson number

$$R_f = \frac{-gD_T(s-1)\partial c/\partial z}{\nu_T(\partial u/\partial z)^2} \tag{38}$$

A larger R_f indicates stronger damping. In the very near-bed region (a few mm from bed), the vertical shear $\partial u/\partial z$ is very large, which is a feature of wave boundary layer, so R_f is a small number, indicating a negligible strat-

ification effect. However, $\partial u/\partial z$ of a wave boundary layer quickly becomes very small at higher levels, e.g. a few cm from the bed, so R_f and hence stratification effect becomes much more significant. As shown in Fig. 5, the predicted c_0 seems to agree well with the measurements for very small z, but the overestimate becomes a factor of 4 for z=1 cm, and then a factor of 15 for $z \sim$3 cm. This, to some extent, suggests that stratification effect decreases with z. Including stratification effect in the present modeling framework possibly requires solving momentum and sediment-diffusion equations by iteration (e.g. Styles and Glenn, 2000), and it can be foreseen that some model parameters must be adopted to allow analytical solutions. Such an extension would require lots of careful research effort, and therefore will be addressed in future studies.

These model validations show that our model works well for large grain size (d_{50} >0.2 mm), which usually does not allow a very significant sediment suspension. However, the prediction can be questionable for fine-sand scenarios (d_{50} <0.2 mm), especially when the net suspended-load transport rate associated with the mean flow is dominant. Thus, in the following model validation, we shall separately consider small (d_{50} <0.2 mm) and large (d_{50} >0.2 mm) grain sizes.

3.2. Net sediment transport rate

In this sub-section, predictions of net sediment transport rate, q_{net}, will be separately evaluated for three factors, i.e. velocity skewness, velocity asymmetry and bottom slope. Some experimental results from previous OWT studies are used for benchmarking, which are summarized in Table 2. The free-streaming velocity for all skewness tests follows the two-harmonic su-

perposition, i.e. Eq. (37). For velocity asymmetry, most validation tests are selected from the dataset reported by van der A et al. (2010) (15 tests with little velocity skewness are chosen), and a typical free-stream velocity, $u_\infty(t)$, for their tests are shown in Fig. 3b. The tests reported by Yuan et al. (2017), in which sinusoidal oscillatory flows are produced over sloping bottoms, are used for testing the prediction of slope-induced q_{net}. Three tests from the experiments reported by Silva et al. (2011) have mixed asymmetric-skewed free-stream flow (their tests C1 to C3), so we also benchmark our model against these results to see if the model can work with the combined effects of net-transport-rate factors.

Our model requires a reference mean velocity as an input, i.e. Eq. (5). The measurements for some selected tests (mostly the asymmetric-flow tests), however, do not include a mean reference velocity. For these tests, we simply define that $u_{cr} = 0$ at z_{cr}=5 cm. This is based on the observation that the mean velocity profiles reported by van der A et al. (2011), which is from the same OWT as van der A et al. (2010), cross zero at roughly $z \sim$5 cm. Change this zero-crossing level by 1-2 cm only slightly affects the final predictions, since the mean-flow-related suspended-load transport rate is of minor importance for asymmetric flows (discussed later in section 3.3). For the slope-effect tests of Yuan et al. (2017), it is assumed that there is no mean flow velocity, since the oscillatory flow is sinusoidal. The model is therefore simplified by neglecting the third-layer of turbulent sediment diffusivity, i.e. $D_T = \kappa u_{*c} z$ in Eq. (20). The YM15 model is also simplified accordingly, so a reference mean velocity is no longer required. We hereafter refer to this as the 2-layer model.

Fig. 6 compares the predicted and the measured q_{net} for large grain sizes (d_{50} >0.2 mm). The predictions are always in the same direction as the measurements, e.g. onshore for skewed and asymmetric flows and offshore (negative or downslope) for slope-effect tests. Also, the agreement is mostly within a factor of 2. To assess the overall model performance, a least-square fit is performed to the data (the dashed lines in Fig. 6), and the obtained slope, A, is used to quantity the overall agreement (A=1 for perfect agreement). The obtained A is 1.01 for skewness, indicating an excellent performance. For asymmetry-induced q_{net}, A is 0.51, suggesting that the model almost underestimate q_{net} by a factor 2. For these tests, the target free-stream $u_\infty(t)$ is used as model input, which is without any velocity skewness. However, as reported by van der A et al. (2010), many tests have some slight skewness, which may result in a larger measured q_{net}. For q_{net} due to mixed asymmetry and skewness, the overall agreement is a factor of 0.76, which is just between those of purely skewed and purely asymmetric flows. For slope-induced q_{net}, the overall agreement is a factor of 0.84, which is similar to that given by the simple model of Yuan et al. (2017).

Fig. 7 shows the model validation for small grain sizes (d_{50} <0.2 mm). For skewed oscillatory flows, it is well understood that the net sediment transport rate can be negative (offshore) for fine-sand scenarios, and our model successfully predict the direction of q_{net} for all tests. It is also encouraging to see that the model accuracy is within a factor of 2 for six of the total eight tests, but the model significantly underestimates q_{net} for the two tests with the largest values of q_{net}. For asymmetry-induced q_{net} (Fig. 7b), the model predicts the observed onshore q_{net} with an overall agreement of 0.51, which

is nearly the same as for large grain sizes. For the slope effect (Fig. 7c), the model underestimates q_{net} by a factor of 0.40, which is slightly over the factor-of-2 threshold.

Based on these results, we conclude that the overall model performance is quite good for large grain sizes, but deteriorates for small gain sizes. To better understand these findings, some details of the model prediction are discussed in the next sub-section.

3.3. Discussions

The total sediment transport rate, q_{net}, consists of bedload ($q_{B,net}$) and suspended-load ($q_{S,net}$) components. Since YM15 model can separate the prediction of mean velocity u_0 into a TI-streaming u_{0s} and a superimposed current u_{0c}, i.e. $u_0 = u_{0s} + u_{0c}$, $q_{S,net}$ can be further separated into three components

$$q_{S,net} = q_{Sw,net} + q_{Ss,net} + q_{Sc,net} \tag{39}$$

where $q_{Sw,net}$ is the wave-related part, $q_{Ss,net}$ and $q_{Sc,net}$ are associated with the TI-streaming and the return current, respectively, i.e.

$$q_{Ss,net} = \int_{z_s}^{\infty} \Phi_{0s} dz = \int_{z_s}^{\infty} u_{0s} c_0 dz \tag{40}$$

and

$$q_{Sc,net} = \int_{z_s}^{\infty} \Phi_{0c} dz = \int_{z_s}^{\infty} u_{0c} c_0 dz, \tag{41}$$

Thus, q_{net} can be divided into one bedload and three suspended-load components. This decomposition will reveal the relative importance of each component, and allow us to better interpret the observed model performance.

We first consider the skewness-induced q_{net}. To this end, test FA7515, for which the model prediction ($q_{net} = -5.5 \cdot 10^{-5} m^2/s$) is within a factor of 2 from the measurement ($q_{net} = -8.8 \cdot 10^{-5} m^2/s$), is selected as an typical example. For this fine-sand test, the suspended-load transport rate dominates, so here we first discuss the three suspended-load components by investigating their associated mean sediment fluxes. As shown in Fig. 8a, the mean fluxes associated with TI-streaming and return current, i.e. Φ_{s0} and Φ_{c0}, are much stronger than Φ_w associated with oscillatory flow. Since the offshore (negative) Φ_{s0} is stronger than the onshore (positive) Φ_{c0} in the very near-bottom region, the total mean flux, Φ, is offshore near the bed, and gradually decays toward zero at higher elevations. Φ_w is onshore near the bed, but becomes offshore around $z = 20$ mm, which suggests that our model indeed captures some phase-lag effect for skewed oscillatory flows. To better understand this, the mean fluxes associated with the leading two harmonics are presented in Fig. 8b, and the predictions of sediment concentration are presented in Fig. 8c (amplitudes) and Fig. 8d (phases). Higher order harmonics are negligible contributors to q_{net} and therefore not shown. The second-harmonic flux is mostly in the onshore-direction, which can be interpreted by the predicted phase of second-harmonic concentration, φ_{c2}. Since the second-harmonic phase of flow velocity, φ_{U2}, varies from about 18° from the bed to 0° outside the wave boundary layer, the sign of $\cos(\varphi_{c2} - \varphi_{U2})$ is mostly determined by φ_{c2}. The predicted φ_{c2} is slightly over 0° at the bottom and decreases to less than -90° until $z \sim$40 mm, where Φ_2 becomes almost zero due to a very small amplitude c_2, so $\cos(\varphi_{c2} - \varphi_{U2})$ and hence Φ_2 is positive. Φ_1, however, starts from an almost zero value near the bed

and becomes increasingly negative (offshore) until reaching a peak around $z = 40$ mm. The predicted φ_{U1} is within 0-18° across the boundary layer. As shown in Fig. 8d, φ_{c1} is -77° at the lowest level, and reduces to -180° until $z \sim$62 mm, so $\cos(\varphi_{c1} - \varphi_{U1})$ is mostly negative for $z <$62 mm, leading to a net offshore $\Phi_1(z)$. A first-harmonic sediment concentration with $\varphi_{c1} - \varphi_{U1}$ between (-90° to -180°) will enhance/reduce the sediment concentration under the negative/positive half-period, corresponding to the well-recognized phase-lag effect.

To reveal the main contributors for q_{net} for skewed oscillatory flows, Fig. 9 presents a bar chart comparing the four components (full colored bars) and the total net transport rate (the hollow bar) for test FA7515. To illustrate the grain-size effect, two more predictions with the same flow condition as FA7515 but larger grain sizes (d_{50}=0.26 mm and 0.39 mm) are also shown. As can be expected from the mean-flux predictions, the dominant components for d_{50} =0.13 mm are $q_{Ss,net}$ and $q_{Sc,net}$, which are one order of magnitude larger than the rests. Since our model overestimates the mean sediment concentration c_0 for this test (Fig. 5b), both $q_{Ss,net}$ and $q_{Sc,net}$ (and their sum) should be overestimated. Nevertheless, these two components, even reduced by a factor of 10, are still quite sizable. The predicted net bedload transport rate, $q_{B,net}$ (magenta bars), is always positive, which is due to the quasi-steady assumption for bedload modeling. The wave-related net suspended-load transport rate, $q_{Sw,net}$ (blue bars), is negative for d_{50} =0.13 mm, which reflects that our model can somehow capture the phase-lag effect. We have concluded that our model overestimated $q_{Ss,net} + q_{Sc,net}$, which is offshore, but the offshore q_{net} is still underestimated. Therefore, it is possible

that the phase-lag effect is underestimated. Many experimental observations show that some residual turbulence at the moment of flow reversal can lead to a significant sediment suspension and therefore enhance the phase-lag effect, but this physics is not included in our model. Another possible reason is that we conceptualize the sediment transport for $z < z_s$ as bedload transport, which is modeled quasi-steadily, while the phase-lag effect may still be present in this thin layer. Future model improvement is required to address these issues. For relatively coarser sand ($d_{50} > 0.2$ mm), the phase-lag effect becomes negligible, e.g. $q_{Sw,net}$ is positive for the two additional predictions, and the net bedload transport rate becomes dominant. These explain why the model performance is better for larger grain size.

For asymmetry-induced q_{net}, we consider a representative test, S706015f, reported by van der A et al. (2010). This test is also with fine sand (d_{50}=0.15 mm), and the free-stream velocity has a maximum of 1.28 m/s and a period of 6 s. The predicted $q_{net} = -4.7 \cdot 10^{-5} m^2/s$ is slightly less than half of the measurement $q_{net} = -10.0 \cdot 10^{-5} m^2/s$. The predictions of mean sediment fluxes and two leading harmonics of sediment concentration are presented in Fig. 10. For asymmetric oscillatory flows in OWTs, both TI-streaming and return current are very weak (see Yuan and Madsen, 2015), so the wave-related flux $\Phi_w(z)$ becomes dominant, as shown in Fig. 10a. The 1st-harmonic flux is the main contributor to $\Phi_w(z)$, i.e. the black dashed line (Φ_1) just deviated a bit from the blue dashed line (Φ_w) in Fig. 10b. Φ_1 is mostly positive (onshore), because the phase φ_{c1} decreases from about 90° near the bottom to -90° at $z \sim$90 mm, leading to a mostly positive $\cos(\varphi_{c1} - \varphi_{U1})$ (φ_{U1} is within 0∼18°). Such values of φ_{c1} will enhance (reduce) the sediment concentration during

the onshore (offshore) half-periods, which agrees with the expected phase-lag effect for asymmetric oscillatory flows. The second-harmonic concentration is mostly determined by the leading first-harmonic time-varying flow, so the prediction is not much different from that for the skewed flow (FA7515 in Fig. 8d). However, the second-harmonic velocity has a phase φ_{U2} about 90°, so 2nd-harmonic velocity and concentration are 90° out-of-phase near the bed, leading to a negligible Φ_2.

The decomposition of q_{net} for the selected asymmetric-flow test is shown in Fig. 11, as well as for two more predictions with coarser gain sizes (d_{50}=0.26 mm and 0.39 mm) but the same flow conditions. A key observation is that $q_{Sw,net}$ is a very important contributor to q_{net}, i.e. it is the dominant one for d_{50} = 0.13 mm. The importance of $q_{Sw,net}$ is also suggested by the experimental results of Ruessink et al. (2011). Since $q_{Sw,net}$ is mainly due to the phase-lag effect, the fact that the model underestimates q_{net} for asymmetric oscillatory flows again suggests that the phase-lag effect is underestimated. For larger grain sizes, the net suspended-load transport rate (mainly due to $q_{Sw,net}$) still carries a heavy weight in the total net transport rate for asymmetric oscillatory flows, which is not true for skewed oscillatory flows. Thus, the model performance for asymmetry is not so good as for skewness, when d_{50} >0.2 mm.

Based on these discussions, we can conclude that our model works well for most cases, except for fine-sand skewed oscillatory flows, when the mean-flow related net suspended-load transport rate is important. The model can reasonably capture but still underestimate the phase-lag effect.

4. Relative importance of net sheet-flow sediment transport rate due to TI-streaming and bottom slope

In this section, we apply the validated model to study whether TI-streaming and bottom slope can lead to significant net sheet-flow sediment transport rate under realistic field conditions. Abreu et al. (2010) proposed the following expression for skewed and asymmetric oscillatory flows under coastal waves

$$u_\infty(t) = U_w f \frac{\left[\sin(\omega t) + \frac{r\sin\phi}{1+\sqrt{1-r^2}}\right]}{[1 - r\cos(\omega t + \phi)]} \tag{42}$$

where U_w is the amplitude, $f = \sqrt{1-r^2}$ is dimensionless factor, r is an index of skewness ($-1 < r < 1$), and ϕ is a phase, which is 0 and $-\pi/2$ for purely asymmetric and purely skewed oscillatory flows, respectively. Ruessink et al. (2009) combined a large dataset of field measurement to study the variation of the two shape parameters, ϕ and r, with the relative wave height H/h, where H is wave height and h is water depth. As shown in their figure 11, the average value of r increases from about 0.2 to 0.6 as H/h decreases from 0.5 to 0.1, while the average value of ϕ changes from about $-\pi/2$ (pure skewness) to about $-\pi/4$ (mixed skewness and asymmetry) for H/h from 0.1 to 0.5. This work and Eq. (42) provide a simple way for constructing a field-condition $u_\infty(t)$ as follows. With a specified wave condition (H/h, T, h), we first estimate the amplitude U_w through the linear wave theory and the three parameters. The shape parameters, ϕ and r, are then taken as the average values reported by Ruessink et al. (2009), which solely depend on H/h. In this way all parameters for $u_\infty(t)$ in Eq. (42) are determined with the information of (H/h,T,h). The obtained $u_\infty(t)$ is converted to a

Fourier series, which is then used as our model input. To isolate the return current, the simplified 2-layer model (discussed in Section 3.2) is used in the following discussion, so it is not necessary to specify a return current. As a result, the net sediment transport rate consists of bedload ($q_{B,net}$), wave-induced ($q_{Sw,net}$) and TI-streaming-induced ($q_{Ss,net}$) suspended-load.

4.1. The importance of TI-streaming

To quantify the importance of TI-streaming-induced $q_{Ss,net}$, we consider the ratio

$$\alpha_{TI} = \frac{|q_{Ss,net}|}{|q_{w,net}|} = \frac{|q_{Ss,net}|}{|q_{B,net} + q_{Sw,net}|} \tag{43}$$

The denominator, $q_{w,net} = q_{B,net} + q_{Sw,net}$, is the net transport rate (bedload plus suspended-load) directly related to the oscillatory flow, and therefore is referred to as the wave-shape-related net transport rate. To assess the typical value of α_{TI}, a case study is conducted as follows. Here we consider coastal waves at a water depth of h=10 m, so a free-stream velocity can be fully determined with H/h and T. To mimic non-breaking coastal waves, H/h is limited to 0.2$\sim$0.4, and T is chosen from 6 s to 12 s. The obtained amplitude of near-bed wave orbital velocity is about 1 to 2 m/s for these flow conditions. For a given sediment diameter d_{50}, a value of α_{TI} can be calculated with specified H/h and T. Since our model performance is not always acceptable for fine sand, here the investigation is based on d_{50}=0.2 mm (medium sand) and 0.4 mm (coarse sand). A Shields parameter ψ_{wmd}, which is given by Eqs. (7) and (8) with $U_b = U_w$ and $k_b = d_{50}$, is also calculated to characterized the flow condition.

Fig. 12 shows the contours for α_{TI} on the H/h-T diagram for the two sediment diameters. Generally speaking, α_{TI} increases with both H/h and

T. This is because the amplitude of near-bed oscillatory flow increases as H/h becomes larger and the water becomes relatively shallower with a larger T, which is reflected by the contours of ψ_{wmd}. As flow condition (represented by ψ_{wmd}) gets stronger, sediment suspension becomes increasingly significant, so the relative importance of $q_{Ss,net}$ increases. Note that the critical ψ_{wmd} for sheet-flow condition is 0.7, according to Madsen (2002). For d_{50}=0.2 mm, α_{TI}=0.2 almost coincides with the contour of ψ_{wmd}=0.7, so at the threshold of sheet-flow condition for this grain size, $q_{Ss,net}$ is not very important. However, α_{TI} increases rapidly with ψ_{wmd}, i.e. α_{TI}=1 when ψ_{wmd} is within 1.2$\sim$1.7, and reaches 10, when ψ_{wmd} becomes 3. Our model probably overestimates $q_{Ss,net}$ for ψ_{wmd}=3, since under this high value of ψ_{wmd} significant sediment suspension possibly leads to the problem of stratification. Nevertheless, it is still believable that $q_{Ss,net}$ becomes dominant under very high values of ψ_{wmd} for medium sand. For the coarse-sand case shown in Fig. 12b and d, the highest value of α_{TI} is only about 0.25, when very large values of H/h and T give a ψ_{wmd} over 2. This suggests that sediment suspension for coarse sand is insignificant under the sheet-flow condition, so there is not enough suspended sand for TI-streaming to produce an important $q_{Ss,net}$.

Based on this simple case study, it can be seen that the TI-streaming can be as important as the wave-shape effect in terms of producing a net sediment transport rate for medium (and possibly fine) sand, but for coarse sand its influence is generally negligible. Since $q_{Ss,net}$ is usually in the offshore-direction, which opposes the usually onshore-directed $q_{w,net}$, TI-streaming and wave-shape effect are competing factors for net sediment transport rate.

4.2. The importance of bottom-slope effect

In this sub-section, we investigate the importance of bottom-slope effect through a case study similar to that for TI-streaming. The field-condition free-stream velocity $u_\infty(t)$ is obtained in the same way described in the last sub-section for h=10m, H/h ∼(0.2∼0.4) and T ∼(6 s∼12 s). A net sediment transport rate for $u_\infty(t)$ over a horizontal bed is first calculated, i.e. $q_{net,nl} = q_{B,net} + q_{Sw,net} + q_{Ss,net}$. Here the TI-streaming effect is included, since it is the result of nonlinear wave shape. In parallel, the net sediment transport rate for a sinusoidal oscillatory flow with the same amplitude U_w and wave period T as $u_\infty(t)$ over a finite bottom slope β is also calculated, i.e. $q_{net,\beta}(\beta)$. By changing the value of β, we find a critical value, β_c, which makes $|q_{net,\beta}(\beta_c)| = |q_{net,nl}|$. In such a way, the critical slope, β_c, which can produce the same magnitude of net sediment transport rate as the wave nonlinearity, is obtained.

Fig. 13 presents the contours of β_c on the H/h-T diagram for the two sediment diameters, d_{50}=0.2 mm and 0.4 mm. Generally speaking, β_c increases with H/h, but the dependency on T is weaker, e.g. some contours are rather horizontal. This is because wave nonlinearity only increases with H/h, so a larger β_c is required to match a stronger net transport rate due to wave nonlinearity. For the medium-sand case (Fig. 13a), β_c is about 3° at the threshold of sheet-flow condition (ψ_{wmd}=0.7), but decreases to less than 1° for ψ_{wmd} between 1.2 and 1.7. This is because $q_{Ss,net}$ and $q_{B,net} + q_{Sw,net}$ almost cancel each other for $\psi_{wmd} \sim$ (1.2 to 1.7) (see the contour of $\alpha_{TI} = 1$ in Fig. 12), so $q_{net,nl}$ is very small. For large value of ψ_{wmd}, the obtained β_c for d_{50}=0.2 mm can reach 20°. This is because a large slope is required to

match a huge $q_{Ss,net}$. For the coarse-sand case (Figure 8b), β_c increases from about 4° when sheet flow just occurs (ψ_{wmd} ~0.7) to over 7° for H/h ~0.4. Generally speaking, this case study shows that a bottom slope between 1 to 10° can be as important as the wave nonlinearity in terms of producing a net sediment transport rate. The actual bottom slope in shallow coastal regions can likely reach these values, and therefore cannot be neglected in modeling net sheet-flow sediment transport rate.

Many practical transport-rate formulas are calibrated without considering the bottom-slope effect, so the immediate question is how to further extend them. The easiest way is to assume that slope effect can be simply superimposed, i.e. adding a $q_{net,\beta}$ which is modeled as a equivalent sinusoidal oscillatory flow with the same root-mean-square velocity over a slope β. In such a way, the extension can be easily achieved by adding a slope-related term. The ways that our model accounts for a bottom slope in fact supports such a linear superposition, which can be shown as follows. According to Yuan et al. (2017), the instantaneous bedload transport rate, ie. Eq. (9), can be approximately written as

$$q_{SB}(t) = q_{SB,0}(t)\left(1 - \frac{\beta(t)}{\tan\varphi_m}\right) \tag{44}$$

where $q_{SB,0}$ is the bedload transport rate on a horizontal bed. We further express $q_{SB,0}$ as

$$q_{SB,0}(t) = q_{SB,0,s}(t) + \Delta q_{SB,0}(t) \tag{45}$$

where $q_{SB,0,s}(t)$ is the bedload transport rate of the equivalent sinusoidal flow and $\Delta q_{SB,0}(t)$ is simply the difference between $q_{SB,0}(t)$ and $q_{SB,0,s}(t)$. The

net bedload transport rate given by time-averaging q_{SB} can be written as

$$q_{B,net} = \overline{q_{SB,0}} - \overline{q_{SB,0,s}\frac{\beta}{\tan\varphi_m}} - \overline{\Delta q_{SB,0}\frac{\beta}{\tan\varphi_m}} \tag{46}$$

where the overbar denotes period averaging. On the right-hand side of Eq. (46), the first term is the net bedload transport rate for the same flow condition over a horizontal bed, while the second term is the slope-induced net bedload transport rate under the equivalent sinusoidal oscillatory flow. The last term is generally much weaker than the first two terms, since wave nonlinearity or a weak current will not make $q_{SB,0}(t)$ dramatically different from $q_{SB,0,s}(t)$, i.e. $\Delta q_{SB,0}$ is much smaller than $q_{SB,0,s}$. Thus, Eq. (46) suggests that the bottom-slope effect on bedload can be modeled independently. For suspended-load prediction, the convective velocity is not affected by bottom slope, and the governing equation for sediment concentration is linear, so we only need to consider the prediction of bottom sediment pick-up rate, $P(t)$. According to Eq. (34), $P(t)$ on a sloping bottom can be written as the product of a horizontal-bed value $P_0(t)$ and a factor $1-\beta(t)/\tan(\varphi_m)$, so we can express $P(t)$ as

$$P(t) = P_0(t) - P_{0,s}(t)\frac{\beta(t)}{\tan\varphi_m} - \Delta P_0(t)\frac{\beta(t)}{\tan\varphi_m} \tag{47}$$

where $P_{0,s}(t)$ is the pick-up rate of an equivalent sinusoidal flow over a horizontal bed and $\Delta P_0 = P_0(t) - P_{0,s}(t)$. The last term is usually negligible, since $\Delta P_0 \ll P_{0,s}(t)$. The first term, $P_0(t)$, will eventually give the net suspended-load transport rate due to wave nonlinearity over a horizontal bed, while the second term will give a net slope-induced suspended-load transport rate that will also occur under the equivalent sinusoidal flow over a slope β. Thus,

the bottom-slope effect on net suspended-load transport rate can also be predicted independently.

As a confirmation, a numerical experiment is designed as follows. For all calculations that give the α_{TI} diagrams in Fig. 12, we add a bottom slope of $\beta = 5°$, and predict a net transport rate $q_{net,full}$, which includes both slope and wave-nonlinearity effects. The difference between $q_{net,full}$, and $q_{net,nl}$ (with β=0) is purely due to bottom slope, i.e.

$$q_{net,\beta}{}' = q_{net,full} - q_{net,nl} \tag{48}$$

Another slope-induced net transport rate $q_{net,\beta}$ is calculated with $\beta = 5°$ and a sinusoidal oscillatory flow with the velocity amplitude U_w and period T used in calculating $q_{net,nl}$ and $q_{net,full}$. The relative difference

$$\varepsilon_\beta = \frac{|q_{net,\beta}{}' - q_{net,\beta}|}{|q_{net,\beta}|} \tag{49}$$

is subsequently calculated. Fig. 14 presents the contours of ε_β on the $H/h-T$ diagram. It can be clearly seen that ε_β increases with H/h. This is because the wave-nonlinear effect increases with H/h, so the interaction between the two effects increases. Nevertheless, the obtained ε_β is generally within 10%. This shows the bottom-slope and the wave-nonlinearity effects on net sheet-flow sediment transport rate can be modeled separately.

It should be noted that the bottom-slope effect in this study is only referred to the effect of bottom-parallel gravity force. As coastal waves shoaling over a sloping bed, wave height may be spatially varying due to the change of water depth, which will result in some spatial variation of near-bed flow and hence sediment transport. This effect will occur over a length scale comparable to the wave length, which is much longer than the excursion amplitude of

near-bed flow. Hence, it is reasonable to believe that the gravity-force effect and the wave-shoaling effect can be independent.

5. Conclusions

In this study, an 1DV process-based model is developed for net sheet-flow sediment transport rate under oscillatory boundary layer flows. The model can rigorously account for two features of wave nonlinearity (velocity skewness and asymmetry) and the bottom-slope effect. Boundary layer hydrodynamics is predicted with the semi-analytical model proposed by Yuan and Madsen (2015), which adopts a time-varying turbulent eddy viscosity. The net bedload sediment transport rate is predicted with the quasi-steady assumption and the bedload predictor of Madsen (1993). The net suspended-load transport rate is given by depth-integrating predictions of net sediment flux in a harmonic-by-harmonic manner. The sediment concentration is predicted by solving the advection-diffusion equation with a turbulent sediment diffusivity based on the flow prediction and a sediment pick-up rate as the bottom condition. The bottom-slope effect on net sediment transport rate is integrated into the process-based model following the concepts proposed by Yuan et al. (2017). For bedload prediction, bottom-parallel gravity force increases (decreases) transport rate in the downslope (up-slope) direction. For suspended-load, sediment pick-up rate is enhanced (reduced) when the flow is in the downslope (up-slope) direction.

The model is able to accurately predict the mean flow embedded in skewed oscillatory flows, which is the residual after the cancellation of a TI-streaming and a return current. The mean sediment concentration is well predicted

when the grain size is relatively large, but is overestimated for fine-sand conditions due to the fact that the model does not account for the stratification-induced turbulence damping. Model validation on net sediment transport rate is separately conducted for three factors leading to a net transport rate, i.e. skewness, asymmetry and slope. The model performance is quite good for large grain size d_{50} >0.2 mm. Only for the asymmetry-induced net transport rate, some moderate underestimate is observed. For small grain size, d_{50} <0.2 mm, the model is able to predict a substantial offshore net transport rate widely observed for skewed oscillatory flows. The model underestimates both asymmetry- and slope-induced net transport rates, but the model performance is still fair. The predicted net transport rate for skewed and asymmetric oscillatory flows in OWTs are decomposed into a bedload and three suspended-load components. Based on two typical flow conditions, it is found that the net suspended-load transport rate dominates for fine-sand scenarios. Under purely skewed oscillatory flows, the mean-flow-related suspended-load component is the main contributor, while the wave-related component dominates under purely asymmetric flows. The fact that our model underestimates the total net transport rate for both skewed and asymmetric flows (when d_{50} <0.2 mm) indicates that the phase-lag effect is underestimated.

To illustrate the relative importance of TI-streaming and bottom-slope effects for producing net sediment transport rate, some computational experiments are conducted. Realistic near-bed oscillatory flows with velocity skewness and asymmetry at a water depth of 10 m is constructed based on the work of Abreu et al. (2010) and Ruessink et al. (2009). A simplified version of the present model, which does not include the current-related component,

is used to predict the net transport rate with the obtained free-stream velocity and a specified bottom slope. The decomposition of net transport rate suggests that the TI-streaming can lead to a net suspended-load transport rate, which can be larger than the net transport rate due to nonlinear wave shape, when significant sediment suspension occurs. A critical bottom slope that gives a net transport rate with the same magnitude as that due to wave nonlinearity effect is calculated. The results suggest that a bottom slope of a few degrees can be equally important as the wave-nonlinear effect. It is found that the slope-induced net transport rate can be independently evaluated for nonlinear oscillatory flows over a sloping bed, which provides a simple way to incorporate the slope effect in existing empirical transport-rate formulas.

Acknowledgments

The authors gratefully acknowledge the financial support from the Tier-1 research project funded by the Ministry Of Education of Singapore (WBS: R-302-000-126-112).

References

van der A, D.A., O'Donoghue, T., Davies, A., Ribberink, J.S., 2011. Experimental study of the turbulent boundary layer in acceleration-skewed oscillatory flow. Journal of Fluid Mechanics 684, 251–283.

van der A, D.A., O'Donoghue, T., Ribberink, J.S., 2010. Measurements of sheet flow transport in acceleration-skewed oscillatory flow and comparison with practical formulations. Coastal Engineering 57, 331–342.

van der A, D. A.and Ribberink, J.S., van der Werf, J., O'Donoghue, T., Buijsrogge, R., Kranenburg, W., 2013. Practical sand transport formula for non-breaking waves and currents. Coastal Engineering 76, 26–42.

Abreu, T., Silva, P.A., Sancho, F., Temperville, A., 2010. Analytical approximate wave form for asymmetric waves. Coastal Engineering 57, 656–667.

Amoudry, L., Hsu, T.J., Liu, P.L.F., 2008. Two-phase model for sand transport in sheet flow regime. Journal of Geophysical Research: Oceans 113, C03011.

Caliskan, U., Fuhrman, D.R., 2017. Rans-based simulation of wave-induced sheet-flow transport of graded sediments. Coastal Engineering 121, 90–102.

Davies, A.G., Li, Z., 1997. Modelling sediment transport beneath regular symmetrical and asymmetrical waves above a plane bed. Continental Shelf Research 17, 555–582.

Dibajnia, M., Watanabe, A., 1992. Sheet flow under nonlinear waves and currents. Proceedings of 23rd International Conference on Coastal Engineering , 2015–2028.

Dohmen-Janssen, C.M., Kroekenstoel, D.F., Hassan, W.N., Ribberink, J.S., 2002. Phase lags in oscillatory sheet flow: experiments and bed load modelling. Coastal Engineering 46, 61–87.

Fuhrman, D.R., Schløer, S., Sterner, J., 2013. RANS-based simulation of turbulent wave boundary layer and sheet-flow sediment transport processes. Coastal Engineering 73, 151–166.

Guizien, K., Dohmen-Janssen, M., Vittori, G., 2003. 1dv bottom boundary layer modeling under combined wave and current: Turbulent separation and phase lag effects. Journal of Geophysical Research: Oceans 108, 3016.

Hassan, W.N., Ribberink, J.S., 2005. Transport processes of uniform and mixed sands in oscillatory sheet flow. Coastal Engineering 52, 745–770.

Hassan, W.N.M., Ribberink, J.S., 2010. Modelling of sand transport under wave-generated sheet flows with a rans diffusion model. Coastal Engineering 57, 19–29.

Herrmann, M., Madsen, O.S., 2007. Effect of stratification due to suspended sand on velocity and concentration distribution in unidirectional flows. Journal of Geophysical Research 112.

Hsu, T.J., Hanes, D.M., 2004. Effects of wave shape on sheet flow sediment transport. Journal of Geophysical Research: Oceans 109, C05025.

Humbyrd, C.J., 2012. Turbulent combined wave-current boundary layer model for application in coastal waters. Master's thesis. Massachusetts Institute of Technology. Cambridge, MA, U.S.

Jimenez, J.A., Madsen, O.S., 2003. A simple forumla to estimate settling velocity of natural sediments. Journal of Waterway, Port, Coastal, and Ocean Engineering 129, 70–78.

King, D.B., 1991. Studies in oscillatory flow bedload sediment transport. Ph.D. thesis. University of California. San Diego, CA, U.S.

Kranenburg, W.M., Hsu, T.J., Ribberink, J.S., 2013a. Two-phase modeling of sheet-flow beneath waves and its dependence on grain size and streaming. Advances in Water Resources .

Kranenburg, W.M., Ribberink, J.S., Schretlen, J.J.L.M., Uittenbogaard, R.E., 2013b. Sand transport beneath waves: The role of progressive wave streaming and other free surface effects. Journal of Geophysical Research: Earth Surface 118, 122–139.

Kranenburg, W.M., Ribberink, J.S., Uittenbogaard, R.E., Hulscher, S.J.M.H., 2012. Net currents in the wave bottom boundary layer: On waveshape streaming and progressive wave streaming. Journal of Geophysical Research 117, F03005.

Li, M., Pan, S., O'Connor, B.A., 2008. A two-phase numerical model for sediment transport prediction under oscillatory sheet flows. Coastal Engineering 55, 1159–1173.

Liu, H., Sato, S., 2006. A two-phase flow model for asymmetric sheetflow conditions. Coastal Engineering 53, 825–843.

Longuet-Higgins, M.S., 1953. Mass transport in water waves. Philosophical Transactions of the Royal Society of London. Series A, Mathematical and Physical Sciences 245, 535–581.

Madsen, O.S., 1991. Mechanics of cohesionless sediment transport in coastal waters, in: Proceedings of Coastal Sediments '91., ASCE. p. pp. 1527.

Madsen, O.S., 1993. Sediment transport outside the surf zone. Technical Report U.S. Army Engineer Waterways Experiment Station.

Madsen, O.S., 2002. Sedment transport outside the surf zone. Coastal Engineering Manual, vol. III. U.S. Army Corps of Engineers, Washington DC. Chapter 6.

Nielsen, P., 1992. Coastal Bottom Boundary Layers and Sediment Transport. World Scientific Publishing.

O'Donoghue, T., Wright, S., 2004. Flow tunnel measurements of velocities and sand flux in oscillatory sheet flow for well-sorted and graded sands. Coastal Engineering 51, 1163–1184.

Ribberink, J., Al-Salem, A., 1994. Sediment transport in oscillatory boundary layers in cases of rippled beds and sheet flow. Journal of Geophysical Research 99, 12707–12727.

Ribberink, J.S., Al-Salem, A.A., 1995. Sheet flow and suspension of sand in oscillatory boundary layers. Coastal Engineering 25, 205–225.

Ribberink, J.S., van der Werf, J.J., O'Donoghue, T., Hassan, W.N.M., 2008. Sand motion induced by oscillatory flows: Sheet flow and vortex ripples. Journal of Turbulence , N20.

Ruessink, B.G., van den Berg, T.J.J., van Rijn, L.C., 2009. Modeling sediment transport beneath skewed asymmetric waves above a plane bed. Journal of Geophysical Research: Oceans 114, C11.

Ruessink, B.G., Michallet, H., Abreu, T., Sancho, F., Van der A, D.A., Van der Werf, J.J., Silva, P.A., 2011. Observations of velocities, sand concentrations, and fluxes under velocity-asymmetric oscillatory flows. Journal of Geophysical Research 116, C03004.

Silva, P.A., Abreu, T., van der A, D.A., Sancho, F., Ruessink, B.G., van der Werf, J., Ribberink, J.S., 2011. Sediment transport in nonlinear skewed oscillatory flows: Transkew experiments. Journal of Hydraulic Research 49, 72–80.

Styles, R., Glenn, S.M., 2000. Modeling stratified wave and current bottom boundary layers on the continental shelf. Journal of Geophysical Research: Oceans 105, 24119–24139.

Sumer, B., Kozakiewicz, A., Fredsøe, J., Deigaard, R., 1996. Velocity and concentration profiles in sheet-flow layer of movable bed. Journal of Hydraulic Engineering 122, 549–558.

Trowbridge, J., Madsen, O.S., 1984. Turbulent wave boundary layers: 2. second-order theory and mass transport. Journal of Geophysical Research: Oceans 89, 7999–8007.

Villaret, C., Davies, A.G., 1995. Modeling sediment-turbulent flow interactions. Applied Mechanics Reviews 48, 601–609.

Watanabe, A., Sato, S., 2004. A sheet-flow transport rate formula for asymmetric, forward-leaning waves and currents. Proceedings of 29th International Conference on Coastal Engineering , 2: 1703–1714.

Wilson, K.C., 1987. Analysis of bed-load motion at high shear stress. Journal of Hydraulic Engineering 113, 97–103.

Wright, S., 2002. Well-sorted and graded sands in oscillatory sheet-flow. Ph.D. thesis. University of Aberdeen. Aberdeen, U.K.

Yu, X., Hsu, T.J., Hanes, D.M., 2010. Sediment transport under wave groups: Relative importance between nonlinear waveshape and nonlinear boundary layer streaming. Journal of Geophysical Research 115, C02013.

Yuan, J., Li, Z., Madsen, O.S., 2017. Bottom-slope-induced net sheet-flow sediment transport rate under sinusoidal oscillatory flows. Journal of Geophysical Research: Oceans 122, 236–263.

Yuan, J., Madsen, O.S., 2015. Experimental and theoretical study of wave-current turbulent boundary layers. Journal of Fluid Mechanics 765, 480–523.

Zyserman, J., Fredsøe, 1994. Data analysis of bed concentration of suspended sediment. Journal of Hydraulic Engineering 120, 121–1042.

Figure captions

Figure 1: Vertical distribution of sediment diffusivity D_T: (a) $D_T = \kappa u_{*c} z$ intersects with the lower two-layer structure at a level below the edge of wave boundary layer δ_w, (b) the intersection is above δ_w.

Figure 2: Definition sketch for reference level $z = 0$, sheet-flow thickness δ_s and erosion depth δ_e: (a) $z' = 0$ is the initial no-motion level, (b) $z = 0$ is the instantaneous no-motion level, which is adopted in the present model.

Figure 3: Examples of free-stream velocity for skewed or asymmetric oscillatory flows.

Figure 4: Prediction of mean velocity profile.

Figure 5: Prediction of mean concentration profile.

Figure 6: Model validation for large grain sizes d_{50} >0.2 mm (solid line: perfect agreement, dotted lines: a factor of 2, dashed lines: least-square fit to data points)

Figure 7: Model validation for fine grain sizes d_{50} <0.2 mm (solid line: perfect agreement, dotted lines: a factor of 2, dashed lines: least-square fit to data points).

Figure 8: Predictions of mean sediment flux and leading two harmonics of sediment concentration for test FA7515.

Figure 9: Decomposition of predicted net sediment transport rate for purely skewed oscillatory flow (test FA7515).

Figure 10: Predictions of mean sediment flux and leading two harmonics of sediment concentration for test S706015f.

Figure 11: Decomposition of predicted net sediment transport rate for purely asymmetric oscillatory flow (test S706015f).

Figure 12: Relative importance of TI-streaming for producing net sediment transport rate. (a) and (c) show the contours of α_{TI} and ψ_{wmd} for d_{50}=0.2 mm. (c) and (d) are similar to (a) and (c) but with d_{50}=0.4 mm.

Figure 13: Relative importance of bottom slope for producing net sediment transport rate. (a) and (c) show the contours of β_c and ψ_{wmd} for d_{50}=0.2 mm. (c) and (d) are similar to (a) and (c) but with d_{50}=0.4 mm.

Figure 14: Relative difference between two predictions of slope-induced net transport rates.

Table 1: Test conditions for benchmarking predictions of mean velocity and concentration

Test ID	$U_{\infty,1}$ [m/s]	$U_{\infty,2}$ [m/s]	T [s]	u_{cr} [cm/s]	z_{cr} [cm]	d_{50} [mm]
C1	0.81	0.26	6.5	1.8	10	0.21
FA7515	1.21	0.31	7.5	-3.0	4.5	0.13

Table 2: Data for benchmarking prediction of net transport rate (N is number of tests)

Reference	Type	N	d_{50} [mm]	T [s]	U_{rms} [m/s]	u_{cr} at z_{cr}
large grain size d_{50} >0.2 mm						
(1) O'Donoghue and Wright (2004)	Skewness	4	0.27, 0.46	5, 7.5	1.25	Yes
(2) Ribberink and Al-Salem (1994)	Skewness	8	0.21	5-12	0.74-1.07	Yes
(3) Hassan and Ribberink (2005)	Skewness	5	0.34	5-12	0.86 1.26	Yes
(4) van der A et al. (2010)	Asymmetry	10	0.27, 0.46	6,7	1.04-1.30	No
(5) Ruessink et al. (2009)	Asymmetry	2	0.20	7	1.16,1.19	No
(6) Yuan et al. (2017)	Slope	16	0.24, 0.51	6.25,8.33	1.06-1.61	No
(7) Silva et al. (2011)	mixed Asy.-Skew.	3	0.2	7, 10	0.86-0.94	No
fine grain size d_{50} <0.2 mm						
(8) O'Donoghue and Wright (2004)	Skewness	2	0.13	5 7.5	1.25	Yes
(9) Hassan and Ribberink (2005)	Skewness	4	0.13	6.5	0.65-1.30	Yes
(10) Wright (2002)	Skewness	2	0.13	4, 6	0.98-1.15	Yes
(11) van der A et al. (2010)	Asymmetry	5	0.15	6,7	1.04-1.30	No
(12) Yuan et al. (2017)	Slope	8	0.13	4.17,8.33	0.9-1.06	No

Figure 1:

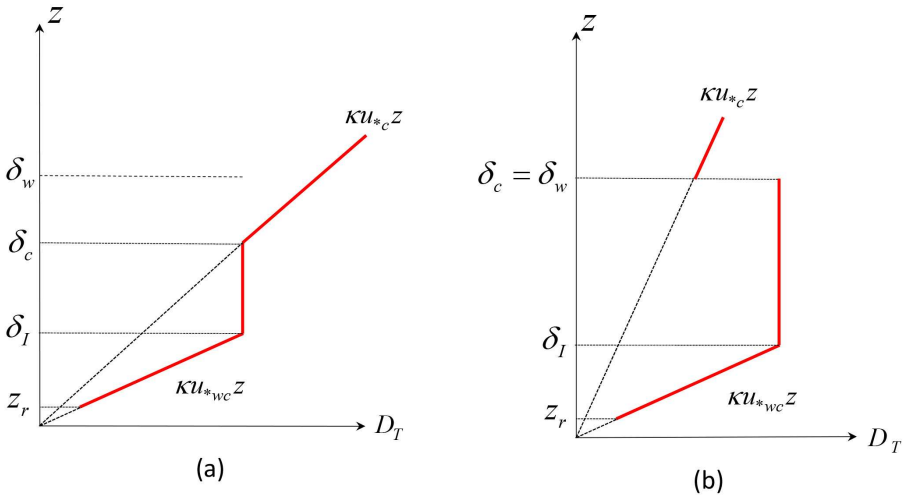

Figure 2:

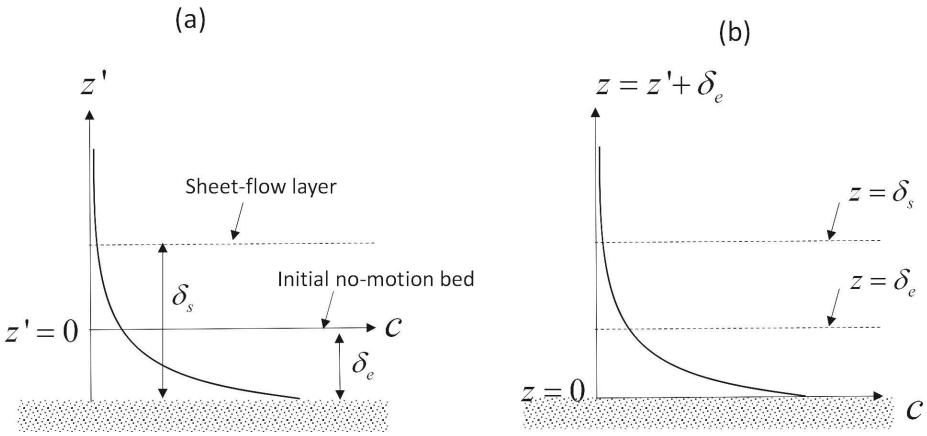

Figure 3:

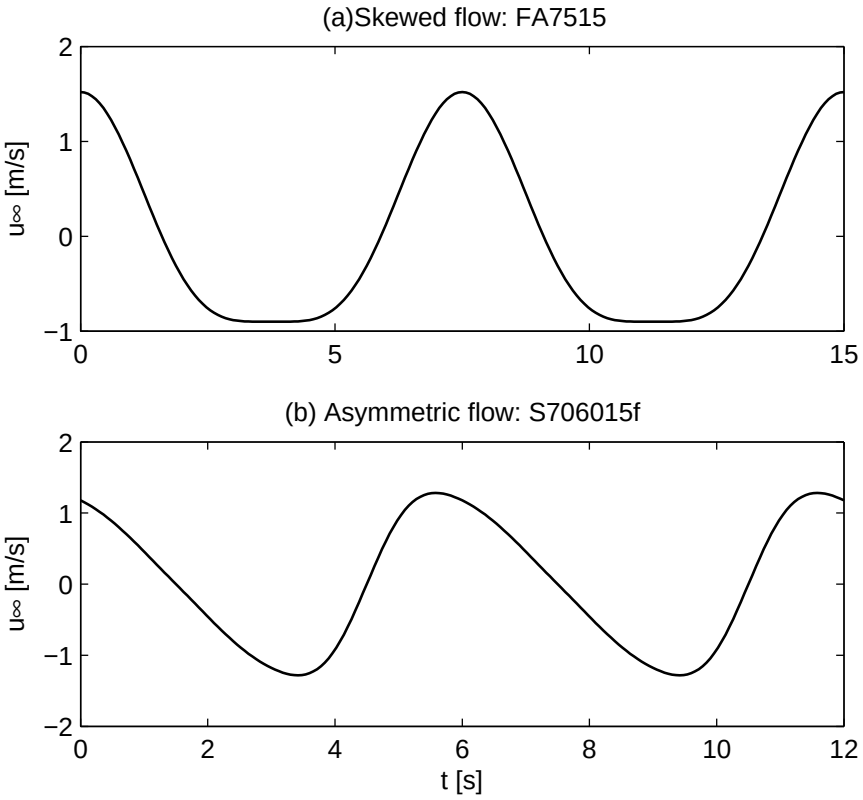
(a)Skewed flow: FA7515
u∞ [m/s]
2
1
0
−1
0
5
10
15
(b) Asymmetric flow: S706015f
u∞ [m/s]
2
1
0
−1
−2
0
2
4
6
8
10
12
t [s]

Figure 4:

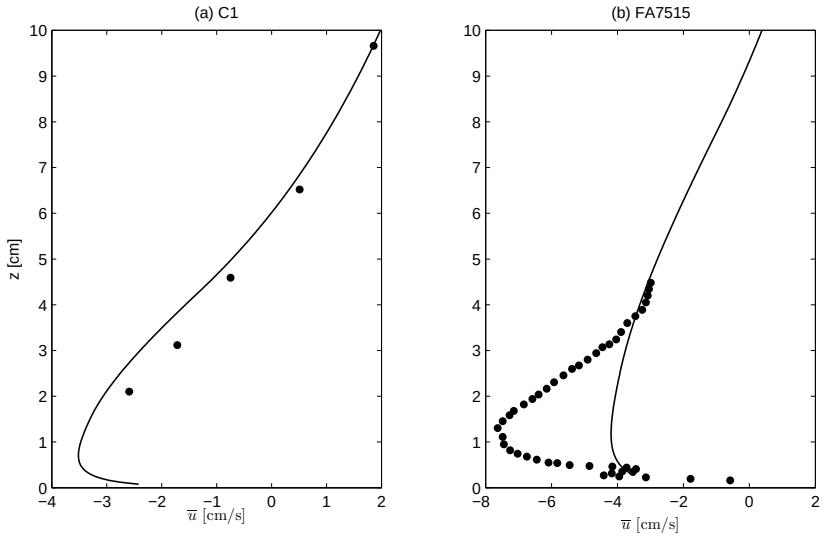

Figure 5:

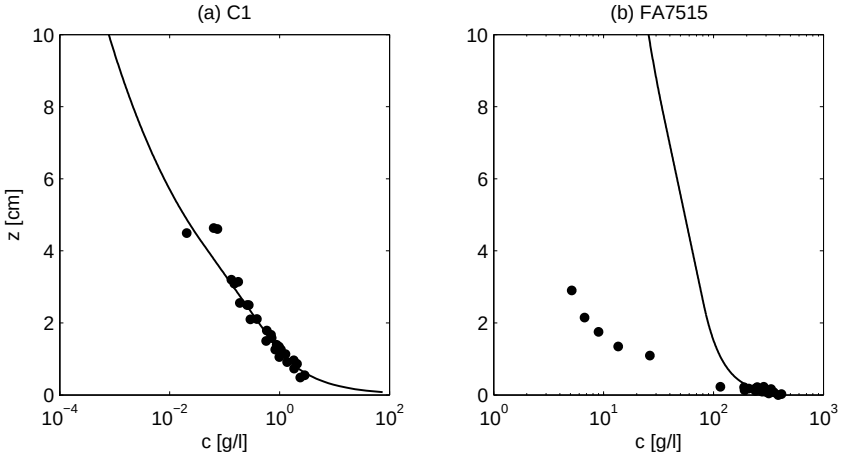

Figure 6:

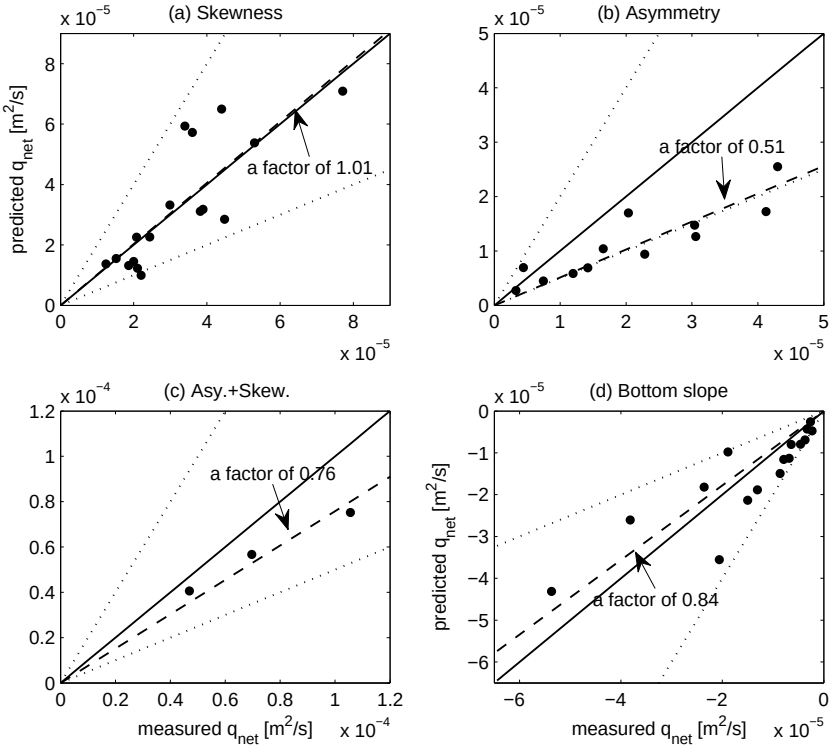
(a) Skewness
x 10^−5
predicted q_net [m^2/s]
a factor of 1.01
x 10^−5
(b) Asymmetry
x 10^−5
a factor of 0.51
x 10^−5
(c) Asy.+Skew.
x 10^−4
a factor of 0.76
measured q_net [m^2/s]
x 10^−4
(d) Bottom slope
x 10^−5
predicted q_net [m^2/s]
a factor of 0.84
measured q_net [m^2/s]
x 10^−5

Figure 7:

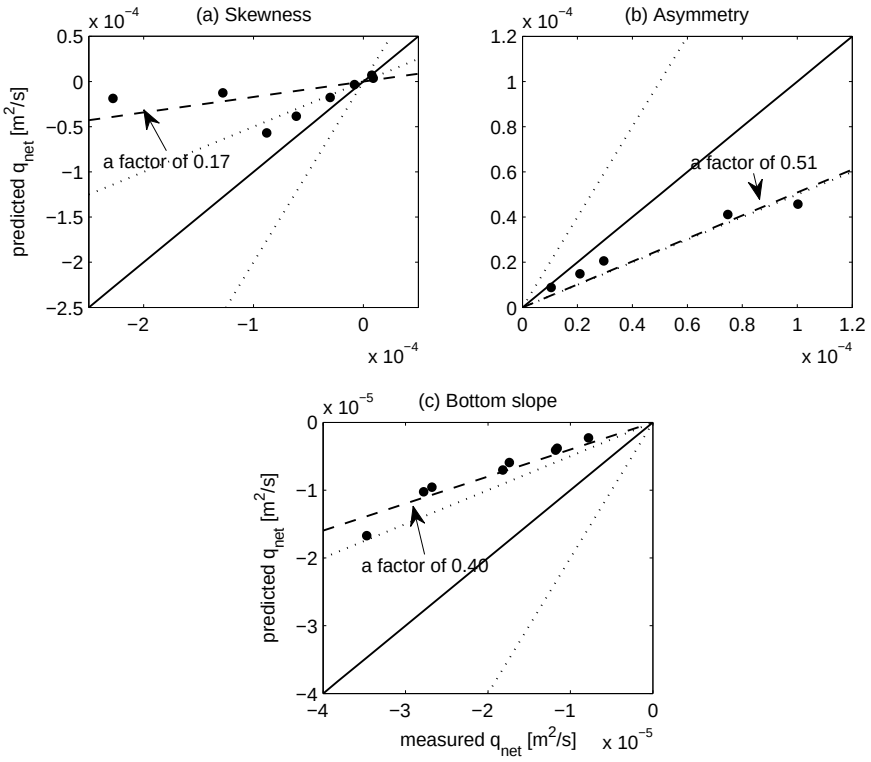
(a) Skewness
x 10^-4
predicted q_net [m^2/s]
a factor of 0.17
x 10^-4
(b) Asymmetry
x 10^-4
a factor of 0.51
x 10^-4
(c) Bottom slope
x 10^-5
predicted q_net [m^2/s]
a factor of 0.40
measured q_net [m^2/s]
x 10^-5

Figure 8:

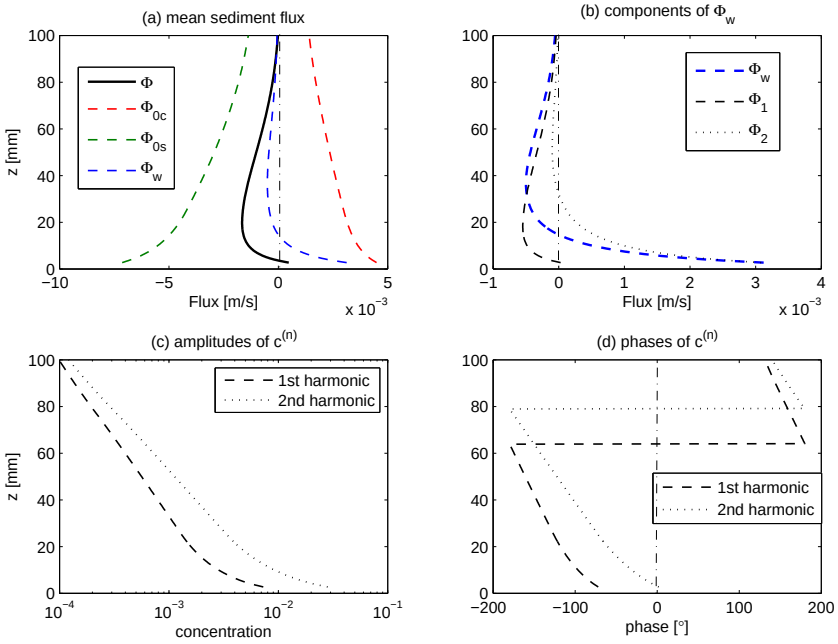
(a) mean sediment flux
z [mm]
Flux [m/s]
x 10^-3
Φ
Φ0c
Φ0s
Φw
(b) components of Φw
Flux [m/s]
x 10^-3
Φw
Φ1
Φ2
(c) amplitudes of c(n)
z [mm]
concentration
1st harmonic
2nd harmonic
(d) phases of c(n)
phase [°]
1st harmonic
2nd harmonic

Figure 9:

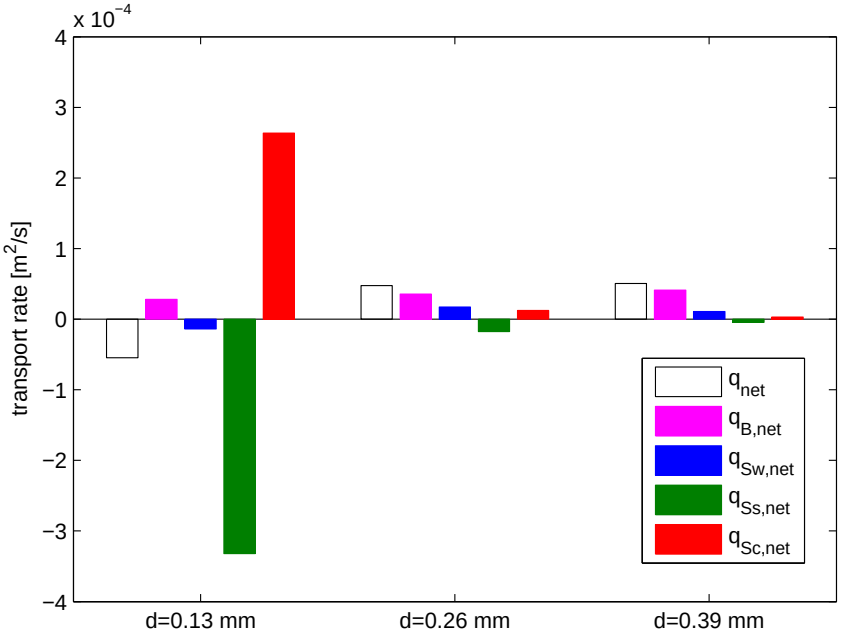
x 10^-4
4
3
2
1
0
−1
−2
−3
−4
transport rate [m^2/s]
d=0.13 mm
d=0.26 mm
d=0.39 mm
q_net
q_B,net
q_Sw,net
q_Ss,net
q_Sc,net

Figure 10:

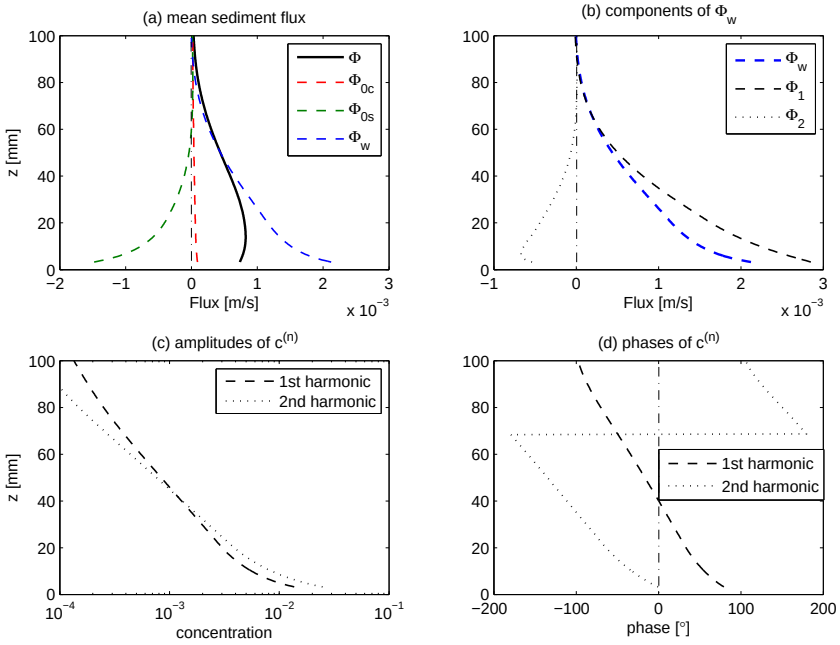
(a) mean sediment flux
z [mm]
Flux [m/s]
x 10^-3
Φ
Φ0c
Φ0s
Φw
(b) components of Φw
Flux [m/s]
x 10^-3
Φw
Φ1
Φ2
(c) amplitudes of c(n)
z [mm]
concentration
1st harmonic
2nd harmonic
(d) phases of c(n)
phase [°]
1st harmonic
2nd harmonic

Figure 11:

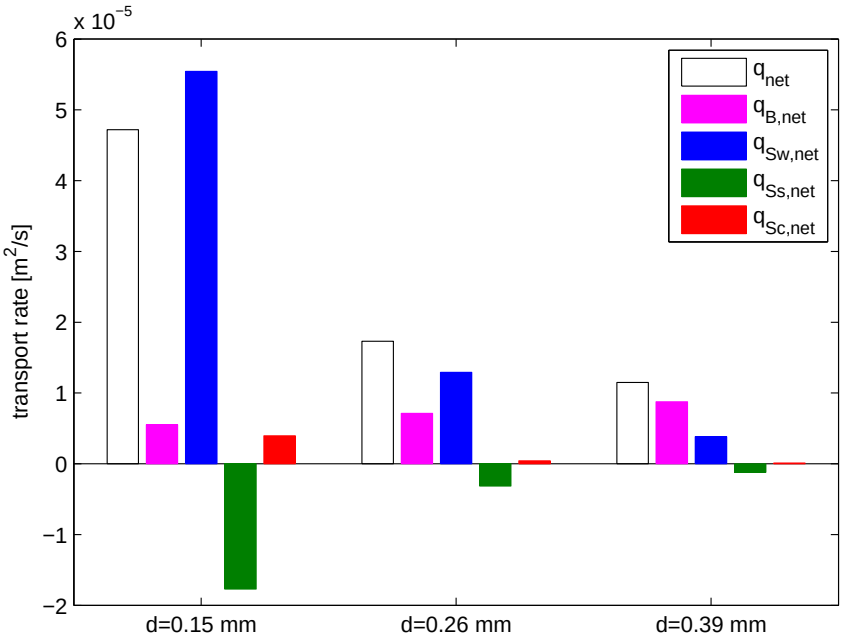
x 10^−5
6
5
4
3
2
1
0
−1
−2
transport rate [m^2/s]
q_net
q_B,net
q_Sw,net
q_Ss,net
q_Sc,net
d=0.15 mm
d=0.26 mm
d=0.39 mm

Figure 12:

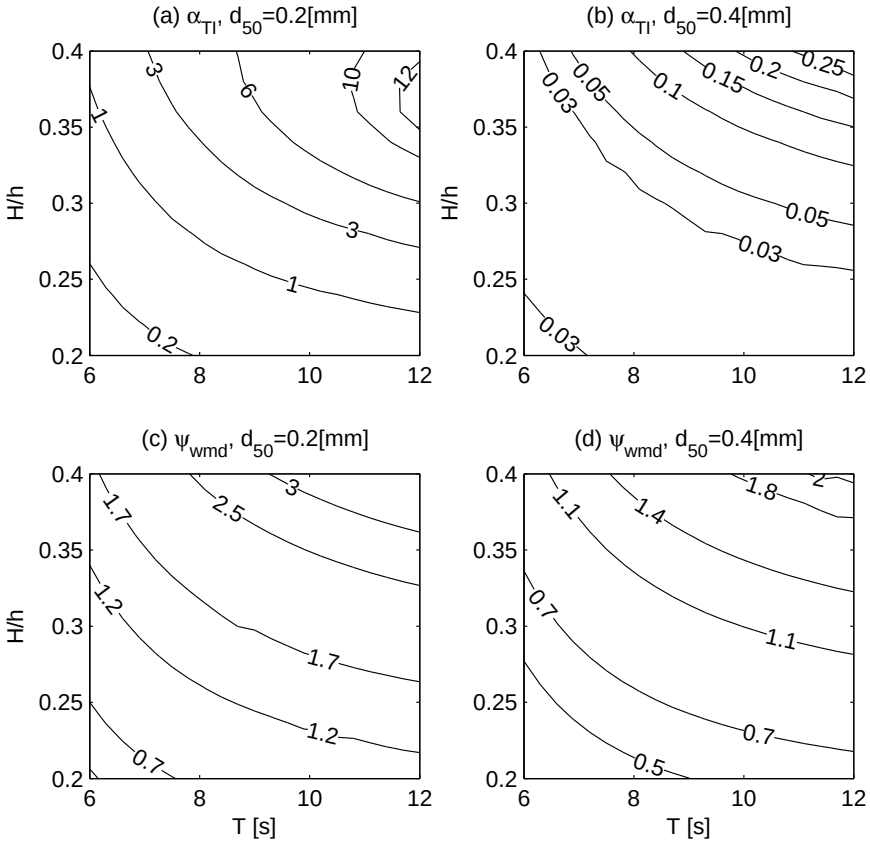
(a) α_{TI}, d_{50}=0.2[mm]
(b) α_{TI}, d_{50}=0.4[mm]
(c) ψ_{wmd}, d_{50}=0.2[mm]
(d) ψ_{wmd}, d_{50}=0.4[mm]
H/h
T [s]
0.4
0.35
0.3
0.25
0.2
6
8
10
12
3
6
10
12
1
3
1
0.2
0.25
0.2
0.15
0.1
0.05
0.03
0.05
0.03
0.03
3
2.5
1.7
1.2
0.7
1.7
1.2
0.7
2
1.8
1.4
1.1
1.1
0.7
0.7
0.5

Figure 13:

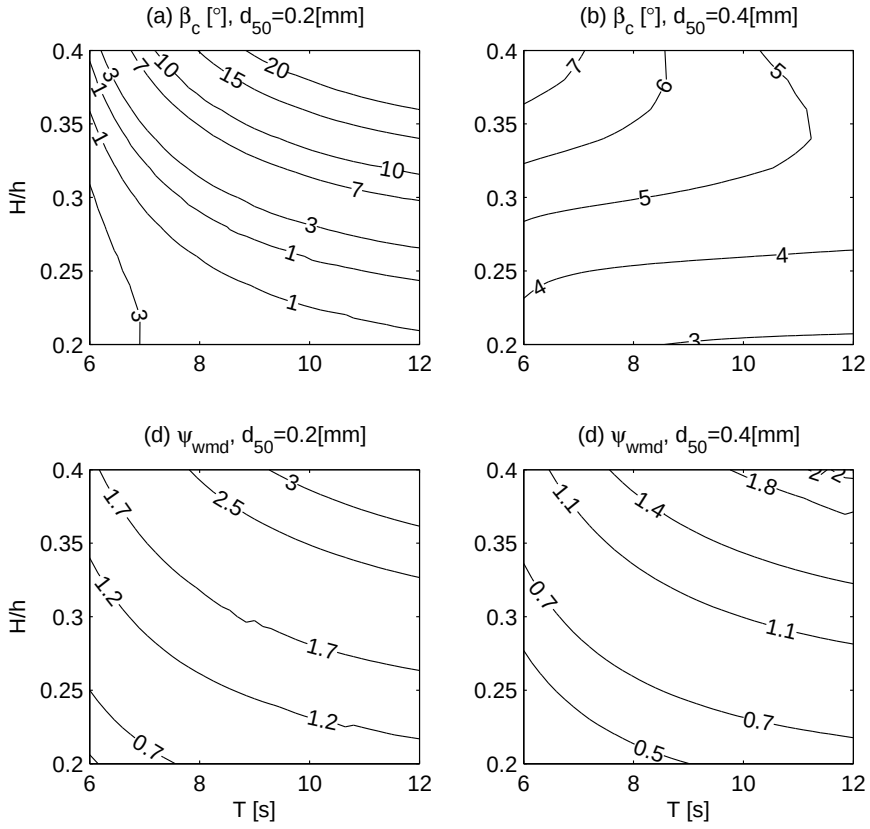

Figure 14:

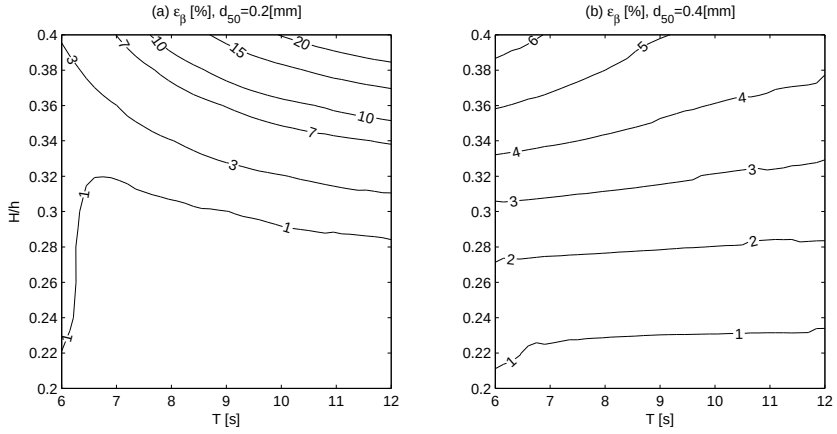

Appendix A. Details of the Yuan and Madsen (2015)'s model

YM15 model adopts the following four-layer structure for the time-averaged turbulent eddy viscosity ν_{T0}

$$\nu_{T0}(z) = \begin{cases} \kappa u_{*wc} z & z_0 \le z < \delta_I \\ \kappa u_{*wc} \delta_I & \delta_I \le z < \delta_J \\ \kappa u_{*wc} \delta_I \exp\left\{-9.5 \frac{z-\delta_J}{\delta_w}\right\} & \delta_J \le z < \delta_K \\ \kappa u_{*c} z & \delta_K \le z \end{cases} \tag{A.1}$$

where κ is the von Karman constant, $\omega = 2\pi/T$ is the wave radian frequency with T being the wave period, $u_{*c} = \sqrt{\tau_{cb}/\rho}$ is the current shear velocity with τ_{cb} being the mean bottom shear stress, u_{*wc} is the period-averaged shear velocity, which is defined as

$$u_{*wc} = \frac{1}{T} \int_0^T \sqrt{\left| \frac{\tau_b(t)}{\rho} \right|} dt \tag{A.2}$$

with $\tau_b(t)$ being the bottom shear stress. The first three layers are within the wave boundary layer and together mimic a parabolic distribution. The first transition layer, δ_I, is defined as $\delta_I = 0.21\delta_w$, where δ_w is the wave boundary layer thickness based on 1%-deficit of free-stream first-harmonic oscillatory velocity. The second transition layer, δ_J, is defined as $\delta_J = 0.79\delta_w$. Above the third transition layer, δ_K, where the current-related $\nu_{T0} = \kappa u_{*c} z$ intersects with the underlying three-layer structure, current becomes dominant. It should be noted that the third layer with an exponentially-decaying ν_{T0} is proposed to avoid δ_K being too large (i.e. far outside the wave boundary layer). This layer only exists if u_{*c} is less than about $1/4\ u_{*wc}$, which indicates an extremely weak current.